Dalton Transactions

Accepted Manuscript

ROYAL SOCIETY OF CHEMISTRY

www.rsc.org/dalton

Cite this: DOI: 10.1039/c0xx00000x

www.rsc.org/xxxxxx

ARTICLE TYPE

Copper Coordinated Ligand Thioether-S and NO_2^- Oxidation: Relevance to Cu_M Site of Hydroxylases

Ram Chandra Maji[a)], Anirban Bhandari[a)], Ravindra Singh[b)], Suprakash Roy[a)], Sudip K. Chatterjee[a)], Faye L. Bowles[c)], Kamran B. Ghiassi[c], Milan Maji [a)], Marilyn M. Olmstead[c)], Apurba K. Patra*[a)]

Received (in XXX, XXX) Xth XXXXXXXXX 20XX, Accepted Xth XXXXXXXXX 20XX

DOI: 10.1039/b000000x

In order to gain insight into the coordination site and oxidative activity of the Cu_M site of hydroxylases such as peptidylglycine α-hydroxylationg monoxygenase (PHM), dopamine β-monoxygenase (DβM), and tyramine β-monoxygenase (TβM), we have synthesized, characterized and studied the oxidation chemistry of copper complexes chelated by tridentate $N_2S_{thioether}$, $N_2O_{sulfoxide}$ or $N_2O_{sulfone}$ donor sets. The ligands are those of *N*-2-methylthiophenyl-2'-pyridinecarboxamide (HL1), and the oxidized variants, *N*-2-methylsulfenatophenyl-2'-pyridinecarboxamide ($HL1^{SO}$), and *N*-2-methylsulfinatophenyl-2'-pyridinecarboxamide ($HL1^{SO2}$). Our studies afforded the complexes $[(L1)Cu^{II}(H_2O)](ClO_4).H_2O$ (**1**.H_2O), $\{[(L1^{SO})Cu^{II}(CH_3CN)](ClO_4)\}_n$ (**2**), $[(L1)Cu^{II}(ONO)]$ (**3**), $[(L1^{SO})Cu^{II}(ONO)]_n$ (**4**), $[(L1)Cu^{II}(NO_3)]_n$ (**5**), $[(L1^{SO})Cu^{II}(NO_3)]_n$ (**6**) and $[(L1^{SO2})Cu^{II}(NO_3)]$ (**7**). Complexes **1** and **3** were described in a prior publication (*Inorg. Chem.*, 2013, **52**, 11084). The X-ray crystal structures revealed either distorted octahedral (in **2**,**4**-**6**) or square-pyramidal (in **1**, **3**) coordination geometry around Cu^{II} ion of the complexes. In the presence of H_2O_2, conversion of **1**→**2**, **3**-**5**→**6** and **6**→**7** occurs quantitatively *via* oxidation of thioether-S and/or Cu(II) coordinated NO_2^- ion. Thioether-S oxidation of L1 also occurs when $[L1]^-$ is reacted with $[Cu^I(CH_3CN)_4](ClO_4)$ in DMF under O_2, albeit low in yield (20%). Oxidation of thioether-S and NO_2^- were monitored by UV-Vis spectroscopy. Recovery of the sulfur oxidized ligands from their metal complexes allowed for their characterization by elemental analysis, ^{1}H NMR, FTIR and mass spectrometry.

Introduction

Peptidylglycine α-hydroxylating monoxygenase (PHM),[1] dopamine β-monoxygenase (DβM)[2] and recently identified tyramine β-monoxygenase (TβM)[3] are copper containing enzymes, that utilizes molecular oxygen as oxidant and catalyze the hydroxylation of a secondary C-H bond of organic substrates for biosynthesis of physiologically active neurotransmitters and hormones.[4,5] The X-ray structure of PHM reveals presence of two copper sites, Cu_M and Cu_H ca. 11 Å apart[1,6,7] as shown in Figure 1. The X-ray structures of Cu_M-X type species, where X = O_2,[6] O_2^{2-} or HO_2^-,[7b] NO_2^-, N_3^- and CO[7a] firmly established that Cu_M site binds substrates, while, the Cu_H site is believed to participate in electron transfer to the Cu_M site during catalytic turnover of the enzyme. That the O_2 binding and activation as well as substrate C-H hydroxylation occurs at the same site, Cu_M, but without Met-S oxidation is unusual. In fact, the choice and role of methionine sulfur (Met-S)[8-10] coordination to Cu_M is still unclear and clearly demands more studies of O_2/H_2O_2 reactivity on thioether-sulfur ligated copper models, which are rare.[11] The only structure of a copper complex, where oxydation of alkyl thioether-S is evident, is of $[(L^{SOEP})Cu^{II}(CH_3OH)(OClO_3)_2]$, reported by Karlin and coworkers.[11h] On the other hand, Cu^{II} mediated aryl thioether-S oxidation is not reported, rather a Cu^{II}-hydroperoxo species formation has been shown by Kodera et al[12] with such type thioether-S donor ligand. Owing to the delocalisation of thioether-S lone pair of electrons to the attached aryl moiety, this sulfur will be less effective to oxidize to sulfoxide (-$(CH_3)SO$) or sulfone (-$(CH_3)SO_2$) following a concomittant reduction of an exogenous substrate such as oxygen.

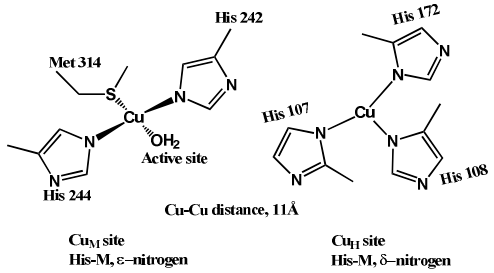

Figure 1. Drawing of the two copper(I) sites in PHM.

Herein, we report the oxidation chemistry of copper complexes of general formulae $[(L1)CuX]_n$, (where HL1 = N-2-methylthiophenyl-2'-pyridinecarboxamide and X=NO_2^- or solvent molecules then n=1 or X=NO_3^-) using *m*-chloroperbenzoic acid (m-CPBA), H_2O_2 and molecular O_2 as oxidants. Using stoichiometric H_2O_2, clean and stoichiometric oxidation of Cu^{II}

coordinated aryl thioether-S and NO_2^- ion to sulfoxide (or sulfone) and NO_3^- respectively are observed. The outcomes of the present investigation demonstrate that the *-trans* effect of a negatively charged donor atom such as amidato N^-, coplanarity of the ligand donors, and *-cis* positioning of thioether-S to the vacant fourth binding site where oxidant possibly binds, enables easy oxidation of aryl thioether-S, following a reaction with H_2O_2. These structural features and consequent thioether-S oxidation for the present set of complexes are in sharp contrast to the structure function of the Cu_M site of hydroxylases. For example, in the precatalytic end-on O_2 bound form, the Cu_M site, maintain distorted tetrahedral geometry and the aliphatic thioether type Met-S is flexible enough to position itself surround Cu_M in such a way (distant most from bound O_2) that Met-S oxidation disfavors, thereby, facilitates only substrate C-H activation and hydroxylation. Ligands employed for the present study are shown in Scheme 1 and the interconversion of various complexes is shown in Scheme 2. Ligand thioether-S and/or NO_2^- oxidation has been monitored by UV-Vis spectroscopy and the isolated products have been characterized by means of various spectroscopic methods including X-ray structures.

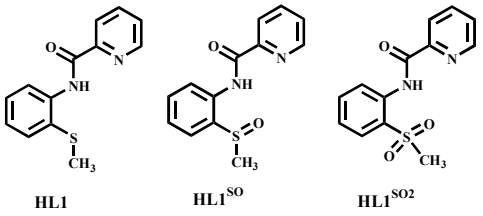

Scheme 1. Ligands employed in this work.

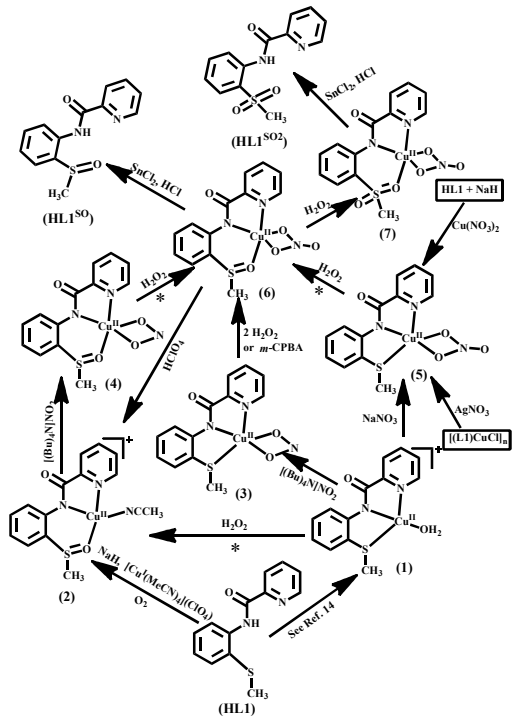

Scheme 2. Schematic presentation of synthesis and interconversion of various complexes. Steps marked with * are monitored by UV-Vis spectroscopy.

Experimental

Reagents and materials

Pyridine-2-carboxylic acid, 2-(methylthio)aniline, triphenylphosphite, sodium hydride, sodium perchlorate, (n-Bu_4N)NO_2, (n-Bu_4N)ClO_4, m-chloroperbenzoic acid (m-CPBA) and H_2O_2 were purchased from Aldrich Chemical Co. and used without further purification. CH_3CN, CH_3OH, $CHCl_3$, CH_2Cl_2, C_5H_5N (pyridine), DMF (dimethylformamide), $(C_2H_5)_2O$ (diethyl ether), n-hexane and n-pentane used either for spectroscopic studies or for syntheses were purified and dried following standard procedures prior to use. The ligand HL1 was synthesized following a reported procedure.[13]

Syntheses

Syntheses of Ligands

HL1 and **$HL1^{SO}$**: Ligand HL1 was synthesized following a reported procedure.[13] Ligand $HL1^{SO}$ was synthesized by the following procedure. Complex **6** (0.05 g, 0.13 mmol) was dissolved in 15 mL of a mixed solvent of CH_2Cl_2 and CH_3CN (1:2 v/v) that resulted in a clear green solution. To this stirred solution $SnCl_2$ (0.293 g, 1.3 mmol) was added. The solution color became yellow, followed by precipitation of a yellow solid. After 10 min stirring, an aqueous solution of 1 mL conc. HCl was added drop wise and the resulting reaction mixture was further stirred for 30 min, then 40 mL diethyl ether was added. The organic layer was washed with distilled H_2O until the water layer was neutral. The organic layer was dried with Na_2SO_4 and kept for slow evaporation that produced white needle shaped crystals of $HL1^{SO}$ (0.029 g, 0.112 mmol, yield = 86%). Elemental analysis calcd for $C_{13}H_{12}N_2O_2S$, **$HL1^{SO}$**: C 59.98, H 4.65, N 10.76; Found: C 59.81, H 4.55, N 10.67; Selected IR frequencies (KBr disk, cm^{-1}): 3278(s, ν_{NH}), 3066(m), 2920(m), 1683(vs, ν_{CO}), 1592(s), 1578(vs), 1514(vs), 1467(m), 1440(s), 1426(s), 1302(s), 1280(m), 1135(w), 1114(m), 1089(m), 1060(m, ν_{SO}), 998(m), 977(m), 942(m), 897(m), 814(m), 749(vs), 691(vs), 621(w), 588(m), 468(m), 402(w). ^1H NMR (500 MHz, $CDCl_3$): δ 11.04 (1H, s, amide-NH), 8.68 (1H, d, pyridine ring proton, J_H 4.6 Hz), 8.56 (1H, d, pyridine proton, J_H 8.25 Hz), 8.29 (1H, d, phenyl ring proton, J_H 7.95 Hz), 7.9 (1H, t, pyridine ring proton, J_H 7.79 Hz), 7.52 (2H, m, phenyl protons), 7.34 (1H, t, pyridine ring proton, J_H 7.81 Hz), 7.26 (1H, s, phenyl proton), 2.44 (3H, s, methyl group of -SMe). EI mass spectrum m/z (%): 543.1($2L1^{SO}$+Na^+, 50), 527.1($2L1^{SO}$ - O + Na^+, 25), 511($2L1^{SO}$ - 2O + Na^+, 100), 283.05 ($L1^{SO}$ + Na^+, 50), 267.05($L1^{SO}$- O + Na^+, 78).

$HL1^{SO2}$: Complex **7** (50 mg, 0.125 mmol) was dissolved in 15 mL of CH_2Cl_2/CH_3CN solvent mixture (1: v/v), and to the solution was added $SnCl_2$ (282 mg, 1.25 mmol). The color of the solution changed from green to yellow with formation of a yellow precipitate. After 10 min, 1mL conc. HCl was added drop wise and stirred for 30 min and diluted with 40 mL ether. The organic layer was washed with distilled H_2O until the water extract was neutral. The organic layer was dried with anhydrous Na_2SO_4, filtered and kept for slow evaporation that afforded white needle shaped crystals of $HL1^{SO2}$ (32 mg, yield = 93%). Elemental analysis calcd for $C_{13}H_{12}N_2O_3S$, **$HL1^{SO2}$**: C 56.51, H 4.38, N

10.14; Found: C 56.43, H 4.23, N 10.08; Selected IR frequencies (KBr disk, cm^{-1}): 3274 (s, amide-NH), 3065(w), 3006(m), 2963(vs), 2921(m), 1698(s, ν_{CO}), 1578(s), 1526(s), 1468(m), 1444(m), 1431(m), 1308(s), 1261(vs, ν_{SO} asymmetric), 1143(s), 1100 (vs, ν_{SO} symmetric), 1016(vs), 970(w), 898(w), 863(w), 800(vs), 763(m), 748(m), 690(m), 676(w), 620(m), 587(m), 550(m), 510(s). 1H NMR (400 MHz, CDCl3): δ 11.75 (1H, s, amide-NH), 8.72 (1H, d, pyridine ring proton, J_H 4.6 Hz), 8.56 (1H, d, pyridine proton , J_H 8.24 Hz), 8.29 (1H, d, phenyl ring proton, J_H 7.96 Hz), 7.9 (1H, t, pyridine ring proton, J_H 7.95 Hz), 7.52 (2H, m, phenyl protons), 7.34 (1H, t, pyridine ring proton, J_H 7.71 Hz), 7.26 (1H, s, phenyl proton), 3.09 (3H, s, methyl group of S−Me). EI mass spectrum m/z (%): 575.1 ({$2L1^{SO2} + Na^+$}, 38), 299.0 ({$L1^{SO2} + Na^+$},75), 277 ({$L1^{SO2} + H^+$},100), 245.08 ({$L1^{SO2}$-2O}, 25).

Syntheses of Complexes

[(L1)Cu(H$_2$O)](ClO$_4$).H$_2$O, 1.H$_2$O and **[(L1)Cu(ONO)], 3:** The synthesis of **3** and **1** was previously reported.[14]

{[(L1^{SO})Cu(CH$_3$CN)](ClO$_4$)}$_n$, 2. Method A: To a stirred CH_3OH solution (9 mL) of **6** (50 mg, 0.13mmol) was added drop wise a CH_3OH solution (10 mL) of 70% $HClO_4$ (37 mg, 0.26 mmol). The clean solution was stirred for 4 hr. Diethyl ether was layered on top of it and kept at -4 ^{0}C. After a day, a green colored compound precipitated out that was filtered and washed with CH_2Cl_2 and dried. The green solid was re-dissolved in CH_3OH/CH_3CN (1:1 v/v) mixed solvent and CH_2Cl_2 was diffused into it to afford needle shaped crystals of **2** suitable for X-ray diffraction (58 mg, 0.125 mmol, yield = 96%). Elemental analysis calcd for $C_{15}H_{14}N_3O_6SClCu$, **2**: C 38.88, H 3.05, N 9.07; Found: C 38.47, H 3.01, N 9.01; Selected IR frequencies (KBr disk, cm^{-1}): 3070(w), 3003(w), 2917(w), 2251(w, ν_{CN} of CH_3CN), 1624(s, ν_{CO}), 1597(s), 1576(s), 1560(s), 1468(s), 1438(w), 1389(m), 1378(m), 1364(m), 1296(m), 1266(w), 1145(vs, $\nu(ClO_4)$), 1119(vs, $\nu(ClO_4)$), 1086(vs, $\nu(ClO_4)$), 984(w, ν_{SO}), 935(w), 813(w), 760(s), 691(w, ν_{CS}), 624(m), 544(w), 499(w), 463(w), 452(w)). Electronic absorption spectrum [λ_{max}, nm (ε, M^{-1} cm^{-1}), in CH_3OH]: 257(13360), 324(7710), 448(232), 685(118).

Method B: To 6 mL DMF solution of HL1 (50 mg, 0.206 mmol) was added solid NaH (4.94 mg, 0.206 mmol). The light yellow solution generated was stirred for 10 min under N_2 atmosphere and then to this solution was added solid [$Cu^I(CH_3CN)_4$](ClO_4) (68 mg, 0.208 mmol). The color of the solution changed from pale yellow to red. After 10 min, O_2 gas was purged to the solution for 15 min and then stirred under O_2 atmosphere for 4 hr. The solution color changed from red to green. The volume of the reaction mixture was reduced to 4 mL and ether was layered on top of this solution and kept at -4 ^{0}C overnight. A dark green sticky mass precipitated out that was dissolved in CH_2Cl_2 and purified by column chromatography on silica gel. The elution with 1:1 v/v CH_3OH/CH_2Cl_2 was evaporated to dryness, redissolved in CH_3CN and kept for slow evaporation that afforded green microcrystals of **2** (21 mg, 20%).

[(L1^{SO})Cu(ONO)]$_n$, 4. Complex **2** (0.15 g, 0.324 mmol) was dissolved in 20 mL CH_3OH to generate a clear green solution. To this solution, solid $NaNO_2$ (0.027 g, 0.391 mmol) or [*n*-Bu)$_4$N]NO_2 (100 mg, 0.347 mmol) was slowly added and the reaction mixture was stirred for 8 hr. The brownish green solution was then kept for slow evaporation, and the resulting needle shaped dark green crystals were filtered off and washed with ether and dried (0.1 g, yield = 84%). Elemental analysis calcd for $C_{13}H_{11}N_3O_4SCu$, **2**: C 42.33, H 3.01, N 11.39; Found: C 42.27, H 2.98, N 11.24; Selected IR frequencies (KBr disk, cm^{-1}): 3078(w), 3059(w), 3020(m), 2928(m), 1619(vs, ν_{CO}), 1597(vs), 1579(vs), 1563(s), 1470(vs), 1439(m), 1439(s), 1371(vs, $\nu(NO_2)$), 1295(m), 1274(m), 1263(m, $\nu(NO_2)$), 1157(m), 1122(s), 1096(m), 996(s, ν_{SO}), 966(m), 945(w), 814(m), 759(s), 691(s, ν_{CS}), 497(m)). Electronic absorption spectrum [λ_{max}, nm (ε, M^{-1} cm^{-1}), in CH_3OH]: 257 (11 188), 320 (6 183), 670 (110).

[(L1)Cu(NO$_3$)]$_n$, 5. Method A: To a stirred solution of **1** (50 mg, 0.113 mmol) in 10 mL CH_3OH solid $NaNO_3$ (12 mg, 0.141 mmol) was added at a time. The resulting reaction mixture was then stirred for 4 hrs and filtered. The filtrate was kept for slow evaporation that afforded needle shaped crystals of **5** after 7 days. The crystals were filtered off and washed with ether and vacuum-dried (33.8mg, yield = 80%). Elemental analysis calcd for $C_{13}H_{11}N_3O_4SCu$, **5**: C 42.33, H 3.01, N 11.39; Found: C 42.07, H 2.93, N 11.28; Selected IR frequencies (KBr disk, cm^{-1}): 3084(w), 3056(w), 3025(w), 2931(w), 1613(s, ν_{CO}), 1590(vs), 1566(vs), 1549(vs), 1467(vs), 1420(w), 1399(m), 1384(vs, $\nu(NO_3)$), 1316(w), 1291(vs, $\nu(NO_3)$), 1276(m), 1147(w), 1092(w), 1048(w), 1026(w), 1014(s, $\nu(NO_3)$), 964(w), 950(w), 900(w), 808(w), 761(m), 751(s), 716(w), 690(m, ν_{CS}), 650(w), 526(w), 477(w), 459(w), 433(w), 420(w). Electronic absorption spectrum [λ_{max}, nm (ε, M^{-1} cm^{-1}), in CH_3OH]: 257 (14 240), 296 (8775), 308 (8 370), 330 (7500), 455 (125), 627 (154).

Method B: To the stirred green solution of [(L1)CuCl]$_n$[14] (0.2 g, 0.584mmol) in 60 mL CH_3CN was added solid $AgNO_3$ (99.24 mg, 0.584 mmol). The clear solution becomes hazy and a white precipitate of AgCl started to precipitate out within few min. The reaction mixture was then stirred for 12 h and filtered through celite pad. The green filtrate was layered with diethyl ether and kept at -10 ^{o}C for a day. The green precipitate was obtained, filtered, and washed with dry diethyl ether. The green solid was dissolved in CH_3OH and kept for slow evaporation. After 6 days bluish green crystals of **5** obtained were filtered off and washed with ether and vacuum-dried (186 mg, yield = 86 %).

Method C: To a stirred CH_3OH solution (10 mL) of HL1 (0.1 g, 0.409 mmol) was added solid NaH (10.86 mg, 0.452 mmol). The resulting light yellow solution of Na(L1) was then added drop wise to a blue solution of $Cu(NO_3)_2.3H_2O$ (104.39 mg, 0.432 mmol). The solution was stirred for 2 hrs. CH_3OH was removed completely under reduced pressure to afford a green solid, which was then dissolved in CH_3CN and kept for slow evaporation. After 4-5 days dark bluish green crystals of **5** were precipitated, filtered off, washed with ether and vacuum dried (104 mg, yield = 69 %).

[(L1^{SO})Cu(NO$_3$)]$_n$, 6. Method A: A solution of **3** (50 mg, 0.141 mmol) in 20 mL CH_3OH was kept in salt/ice bath (~ -12 ^{0}C). To this stirred solution a diluted solution (4 mL CH_3OH) of 17 µl of

50% H_2O_2 (0.29 mmol) was added drop wise. The color of the solution changed from bluish green to dark green. The solution was stirred for 4 hr. and then the volume of the solution was reduced to 3 mL using rotary evaporator. Diethyl ether was layered to this concentrated solution and kept at -4 ^{0}C. After 2 days, a fluorescent green compound was precipitated, filtered off, washed with ether, and dried. This green residue was re-dissolved in CH_2Cl_2 and pentane diffused into this solution to afford needle shaped crystals suitable for X-ray diffraction studies after 3 days (40 mg, yield = 74%). Elemental analysis calcd for $C_{13}H_{11}N_3O_5SCu$, **6**: C 40.57, H 2.88, N 10.92; Found: C 40.17, H 2.78, N 10.68; Selected IR frequencies (in KBr disk, cm^{-1}): 3078(w), 3014(w), 2923(w), 2856(w), 1621(s, ν(CO)), 1598(m), 1578(w), 1564(m), 1466(vs), 1435(w), 1384(vs, $\nu(NO_3)$), 1374(m), 1307(w), 1291(s, $\nu(NO_3)$), 1268(w), 1149(w), 1124(w), 1052(w), 1015(w), 992(m, ν_{SO}), 760(m), 691(m, ν_{CS}), 649(w), 536(w), 499(w), 466(w), 449(w). Electronic absorption spectrum [λ_{max}, nm (ε, M^{-1} cm^{-1}), in CH_3OH]: 257(10 580), 324(5 840), 438(197), 668(91).

Method B: Complex **3** (150 mg, 0.425 mmol) was dissolved in 20 mL CH_2Cl_2 and then the solution was cooled down to -10 °C using salt/ice bath. To this cooled, vigorously stirred solution was then added *m*-CPBA (75 mg, 0.435 mmol) pinch wise. The color of the solution changed from bluish green to dark green. The solution was then stirred for 3hrs at room temperature and to this was then layered 30 mL of hexane and kept at -4 ^{0}C. After 12 hr, fluorescent green compound was precipitated, filtered off and washed with hexane, ether and dried. This green solid was recrystallized dissolving in CH_2Cl_2 and then pentane diffusion at room temperature to afford needle shaped crystals of **6** (75 mg, 45% yield).

[($L1^{SO2}$)Cu(NO_3)], 7: Complex **6** (200 mg, 0.52 mmol) was dissolved in 6 mL CH_3OH and the resulting green solution was then cooled to -10 ^{0}C under N_2. To the stirred solution was then added CH_3OH solution (1 mL) of 29 µL of 50% H_2O_2 (0.52 mmol) drop wise. Solution was stirred for 4 hr at -10 ^{0}C and then stirred overnight at room temperature. The resulting reaction mixture was kept for slow evaporation to afford green microcrystals after 7 days (160 mg, yield = 76%). Elemental analysis calcd for $C_{13}H_{11}N_3O_6SCu$, **7**: C 38.95, H 2.74, N 10.49; Found: C 38.75, H 2.58, N 10.18; Selected IR frequencies (in KBr disk, cm^{-1}): 3075(w), 3028(w), 3000(w), 2926(w), 1623(s, ν(CO)), 1593(s), 1578(m), 1565(s), 1471(s), 1439(w), 1384(vs, $\nu(NO_3)$), 1296(s, $\nu(NO_3)$), 1265(m), 1140(m, $\nu(SO_2)$ asymmetric), 1116(w), 1097(m, $\nu(SO_2)$ symmetric), 1066(w), 1043(w), 1005(w), 957(w), 758(s), 691(m, ν_{CS}), 649(w), 553(w), 490(w), 458(w), 433(w). Electronic absorption spectrum [λ_{max}, nm (ε, M^{-1} cm^{-1}), in CH_3OH]: 248(7545), 300(4720), 692(81).

Synthesis safety note

Transition metal perchlorates are hazardous and explosive upon heating and should be handled cautiously. No explosion occurred in the present study.

Physical measurements

The FTIR spectra of the ligand and the complexes were recorded on a Thermo Nicolet iS10 spectrometer using KBr pellet in the range 4000 – 400 cm^{-1}. The electronic spectra were recorded on an Agilent 8453 diode array spectrophotometer. Elemental analyses were carried out on a Perkin-Elmer 2400 series-II CHNS Analyzer. Mass spectra were recorded on Waters-HAB213 spectrometer. Solution conductivity was measured using CHEMILINE conductivity meter CL220, ^{1}H NMR spectra were recorded on JEOL JNM LA 400 and JEOL JNM LA 500. Electron paramagnetic resonance (EPR) spectra were obtained using Bruker-EMX-1444 EPR spectrometer. Redox potentials were measured using CHI 1120A potentiometer.

Cyclic voltammetry

Redox potentials were measured using CHI 1120A potentiometer. Three electrode cell set up such as platinum, saturated calomel and a platinum wire as a working, reference and auxiliary electrode respectively have been used for the measurements. All the potentials reported are *vs* SCE and measurements were carried out under nitrogen atmosphere.

Crystallography

Crystal structures of **1** and **3** were reported previously. Crystals suitable for X-ray diffraction of **4** and **5** were grown by slow evaporation of CH_3OH or CH_3CN solution of the complexes respectively. Crystals of **6** were grown by pentane diffusion into a CH_2Cl_2 solution of **6** whereas for **2**, CH_2Cl_2 was diffused into a solution of this compound in a mixed solvent of CH_3OH/CH_3CN (1:1 v/v). Single crystal intensity measurements for **3-6** and **1-2** were collected at 90(2) K with a Bruker Smart APEX II CCD area detector using MoKα radiation (λ = 0.71073 Å) with a graphite monochromator (for **2**, **4** and **5**) or synchrotron radiation with a Silicon 111 monochromator (for **6**). The cell refinement, indexing and scaling of the data set were carried out using SAINT and Apex2 programs.[15] All structures were solved by direct methods with SHELXS, and refined by full-matrix least square based on F^2 with SHELXL.[16] The perchlorate anion present in **2** is not disordered. The positions of the C-bound H atoms were calculated assuming ideal geometry and refined using a riding model. Figures showing displacement parameters were created using the program XP[17]. Crystal data for the complexes **2** and **4-6** are summarized in Table 1. Additional crystallographic data and refinement details are available in CIF format in the Supporting Information.

CCDC reference numbers for **4**, **5**, **6** and **2** are 1402244-1402247 respectively.

Results and discussion

Syntheses and characterisation

Ligand HL1 was prepared following reported procedures[13] and characterized by ^{1}H NMR, Mass and FTIR spectrum (ν_{N-H} at 3278 cm^{-1} and $\nu_{C=O}$ at 1682 cm^{-1}). The ligand $HL1^{SO}$ displays ν_{NH} at 3278 cm^{-1}, ν_{CO} at 1683 cm^{-1} and a strong, broad absorption centered at 1060 cm^{-1} due to ν_{SO} whereas $HL1^{SO2}$ displays ν_{NH} at 3274 cm^{-1}, ν_{CO} at 1698 cm^{-1} and $\nu_a(SO_2)$ at 1261 cm^{-1} and $\nu_s(SO_2)$ at 1100 cm^{-1} correspond to asymmetric and symmetric stretching respectively.[18] Presence of molecular ion peak at m/z =

277 in the mass spectrum of $HL1^{SO2}$ strongly corroborates its formulation (Supporting Information). Also the lower field chemical shift of the methyl proton at δ = 3.09 ppm as compared to that of $HL1^{SO}$ which is at δ = 2.44 ppm supports formation of $-SO_2(CH_3)$ moiety in the ligand frame upon H_2O_2 treatment to the CH_3OH solution of **6**. A strong base, NaH has been used to deprotonate the amide proton of the ligands prior to their reaction with starting metal salt. The absence of ν_{N-H} and the red shifted ν_{CO} of **2** (1624 cm^{-1}), **4** (1619 cm^{-1}), **5** (1613 cm^{-1}), **6** (1621 cm^{-1}) and **7** (1623 cm^{-1}) compared to the corresponding free ligands confirm the amidato N^- ligation to Cu ions in these complexes. Addition of either equivalent amount of $[n\text{-}Bu_4N]NO_2$ or excess $NaNO_2$ to a CH_3OH solution of **2** afforded **4** in high yield. The IR spectrum of **4** displays strong stretches at 1371 cm^{-1} and 1263 cm^{-1} those correspond respectively to the $\nu_a(NO_2)$ and $\nu_s(NO_2)$.[18] The medium intense stretches at 984 cm^{-1}, 996 cm^{-1} and 992 cm^{-1} observed in the IR spectrum of **2**, **4** and **6** respectively are due to the ν_{SO} of the O-coordinated sulfoxide group of ligand $HL1^{SO}$, which are comparable to the reported values (Supporting Information). IR spectrum of **7** displays stretches at 1140 cm^{-1} and 1097 cm^{-1} those correspond to the $\nu_a(SO_2)$ and $\nu_s(SO_2)$ vibrations of the sulfone ($-SO_2$) group (Supporting Information).

Solution conductivity measurements in CH_3CN reveal that, except **2,** all other complexes, **4-7,** are non-electrolytic (Λ ranges from 7-13 Ω Mol^{-1} cm^{-1}) whereas **2** behaves as 1:1 electrolyte (Λ ranges from 136 Ω Mol^{-1} cm^{-1}).[19] Mass spectral results, microanalytical data along with other spectroscopic information support the formulations of the complexes as given.

Crystal structures

Structures of the complexes

The reported X-ray structures of$[(L1)Cu^{II}(H_2O)](ClO_4).H_2O$, **1** and $[(L1)Cu^{II}(ONO)]$, **3** feature distorted square pyramidal (SPY) geometry around Cu^{II} ion with a trigonality index τ value[20] of 0.11 and 0.13 respectively.[14] The structures of **2**, **4**, **5** and **6** are depicted in Figures 2-5. Three donors of the $N_2S_{thioether}$ donor tri-dentate mono-carboxamide ligand, L1, occupy three sites of the square plane of which the amidato N^- donor is *-trans* to the fourth site of the plane. The remaining two positions are occupied by the two O atoms, one of a water molecule (square plane) and other of one ClO_4^- anion (axial) in case of **1** or the two O atom of the bound nitrite anion (NO_2^-) in case of **3**.[14] In compound $[(L1)Cu^{II}(NO_3)]_n$,**5**, ligand L1, as the parent thioether, provides N_2S chelation. In compounds $\{[(L1^{SO})Cu^{II}(CH_3CN)](ClO_4)\}_n$, **2**, $[(L1^{SO})Cu^{II}(ONO)]_n$,**4** and $[(L1^{SO})Cu^{II}(NO_3)]_n$, **6**, where the thioether has been oxidized to a sulfoxide ($L1^{SO}$), chelation occurs through a N_2O donor set. A fourth coordination site is occupied by acetonitrile in **2**, nitrite in **4**, and nitrate in **5** and **6**. However, the Cu coordination environment and geometry could be considered to be 4+2, distorted octahedral (Oh) in **2** and **4**-**6**. Each of these four structures is a chiral polymer. In compound **3**, and also in compound **4**, the nitrite group is asymmetrically bound, with one oxygen more distant from the metal. This is the typical arrangement for O-nitrito coordination. The plane of the O-N-O group is close to perpendicular to the metal ligand plane, subtending a dihedral angle of 80.00(8) ° in **3** and 86.92(12)° in **4**. An apparent structural *-trans* effect is evident in compound **5**. The bond that is *-trans* to the bonded thioether-S is longer, Cu-N = 2.0156(14) Å, than the bond that is *-trans* to O in the sulfoxide species, which have an average Cu-N distance and average deviation of 1.994(7) Å. The polymer is propagated by Cu coordination to the C=O oxygen of the neighboring complex, forming the 5th bond to Cu (Supporting Information). The more elongated sixth coordination site comes from the anion: either a long distance interaction from the coordinated nitrite or nitrate, or from a perchlorate oxygen. The $Cu\text{-}O_{(SO)}$ distances of 1.9948(15) Å, 1.9742(18) Å and 1.963(3) Å and the sulfoxide S-O distances of 1.5334(16) Å, 1.5291(19) Å and 1.536(3) Å respectively for **2**, **4** and **6** have been observed. These S-O distances observed are in accord to that of reported complexes where sulfoxide O coordination to metal center occurs.[12h-i,20] When the sulfoxide is coordinated to metal ion through its S donor, a much shorter S-O distance (1.472 Å) is observed than that when it is coordinated via its O donor atom (1.5418 Å).[21,22] However, no example of structurally characterized copper complexes with sulfoxide S donor is yet known. This occurrence of longer S-O distance for the O coordinated sulfoxide is also reflected in the IR spectrum of these complexes. These display red shifted SO stretching vibrations (ν_{SO} ~990 cm^{-1}) relative to the sulfoxide S-bound (ν_{SO} ~1150 cm^{-1}) coordination.[22] The stronger coordination of the amidato N^- to Cu^{II} is evident in all cases, therefore, the $Cu^{II}\text{-}N_{amide}$ distances (in the range 1.9378 Å-1.983 Å) in **2** and **4**-**6** are shorter than the $Cu^{II}\text{-}N_{py}$ distances (in the range 1.988 Å-2.0156 Å) in the respective complexes.

The pyridine and phenyl rings of L1 or $L1^{SO}$ are not coplanar. The twist angle between the ring planes of 50.28^0, 46.25^0, 38.03^0 and 44.12^0 have been observed for the octahedral complexes, **2** and **4**-**6** respectively. The striking differences in the structure of **1**, **3** and **5**, where parent thioether-S chelation is there, are the Cu-S distances [for **1**: 2.3126(5) Å, for **3**: 2.2875(11) Å and 2.3004(12) Å and for **5**: 2.4546(4) Å] and the twist angle between the two ring planes of the ligand [for **1**: 3.87^0, for **2**: 7.64^0 and for **5**: 38.03^0]. These significant structural differences, particularly the elongation of Cu-S bond, is more likely due to the geometry difference around Cu^{II} ion, SPY in **1** and **3** versus Oh in **5**. In native PHM structure where Cu_M has a distorted tetrahedral geometry, the average $Cu\text{-}N_{His}$ distance of 2.025 Å, $Cu\text{-}O_{water}$ of 2.00 Å and $Cu\text{-}S_{Met}$ of 2.68 Å is observed.[1a] Quite interestingly a large variation of $Cu\text{-}S_{Met}$ distance in the range of 2.38 Å -2.68 Å is known from the X-ray structure of PHMs.[1a-b,6,9] In **1** the average Cu-N distance of 1.9582(12) Å, $Cu\text{-}O_{water}$ of 1.9551(11) Å and $Cu\text{-}S_{thioether}$ of 2.3126 Å was observed.[14] Furthermore, in **3**, an asymmetric nitrite binding to Cu^{II} is evident with an average longer $Cu\text{-}O_{nitrite}$ distance of 2.610(2) Å and shorter $Cu\text{-}O_{nitrite}$ distance of 1.9717(19) Å, like found for the NO_2^- bound Cu_M site of reported PHM structure,[7a] where these distances are of 2.6 Å and 1.9 Å respectively. The τ value of 0.13 for **3** and 0.22 for nitrite bound Cu_M site of PHM reveals a distorted SPY coordination geometry around Cu^{II} in both cases. The cationic part view of **2** and the perspective full molecule view of **4**-**6** are shown in Figures 2-5, respectively, with their atom labeling schemes. Selected bond distances and angles are tabulated in Table 2.

Table 1 Data collection and structure refinement parameters for the complexes **2** and **4-6**

Complex	**2**	**4**	**5**	**6**
formulae	$C_{15}H_{14}N_3O_6SCl Cu$	$C_{13}H_{11}N_3O_4S Cu$	$C_{13}H_{11}N_3O_4S Cu$	$C_{26}H_{22}N_6O_{10}S_2 Cu_2$
mol wt.	463.34	368.85	368.85	769.70
Crys system	monoclinic	orthorhombic	orthorhombic	triclinic
Color	green	green	green	green
Space group	$P2_1$	$P2_12_12_1$	$P2_12_12_1$	$P1$
a (Å)	8.8284(12)	8.1038(6)	7.1023(3)	7.77240(14)
b (Å)	8.0746(11)	8.6948(7)	9.1422(3)	9.2706(17)
c (Å)	12.3897(16)	20.2700(15)	20.9440(8)	10.851(2)
α (°)	90.0	90.0	90.0	105.763(2)
β (°)	99.540(2)	90.0	90.0	101.288(2)
γ (°)	90.0	90.0	90.0	90.422(3)
V (Å^3)	871.0(2)	1426.24(19)	1359.91(9)	736.39(19)
Z	2	4	4	1
d_{calc}(g cm^{-3})	1.767	1.715	1.802	1.736
θ range, deg	2.34-30.65	2.5-27.5	2.43-30.59	3.26-29.78
μ (mm^{-1})	1.567	1.696	1.782	2.090
F(000)	470	748	748	390
refl./params.	13792/247	15987/200	21518/200	8491/417
unique refl.	5344	3290	4161	6004
R_1 [I>2σ(I)][a]	0.0198	0.0213	0.0158	0.0438
wR_2 [I>2σ][b]	0.0491	0.0541	0.0422	0.1142
GOF	1.040	1.111	1.038	1.022
res. dens. eÅ^{-3}	0.316/-0.293	0.539/-0.305	0.339/-0.200	0.850/-0.983

[a] $R = \sum||F_o| - |F_c||/\sum|F_o|$
[b] $wR_2 = \{\sum[w(F_o^2 - F_c^2)^2] / \sum w[(F_o^2)^2]\}^{1/2}$

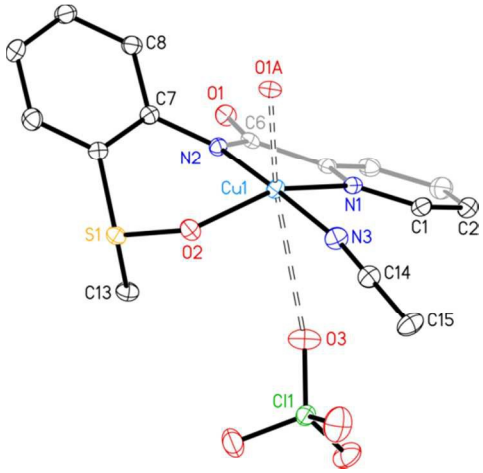

Fig 2. Thermal ellipsoid (probability level 50%) plot of {[(L1^{SO})Cu(CH$_3$CN)](ClO$_4$)}$_n$, **2** with the atom labeling scheme. H atoms are omitted for the sake of clarity.

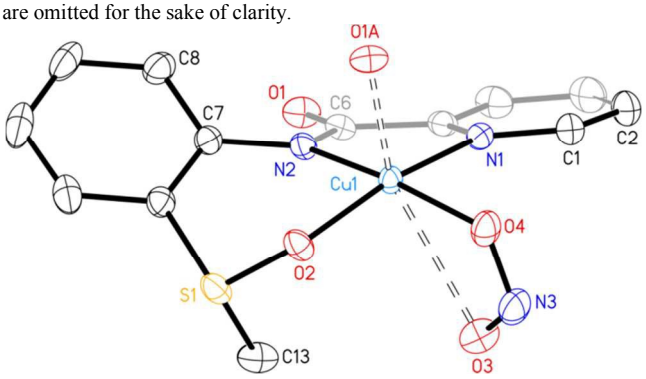

Fig 3. Thermal ellipsoid (probability level 50%) plot of [(L1^{SO})Cu(ONO)]$_n$, **4** with the atom labeling scheme. H atoms are omitted for the sake of clarity.

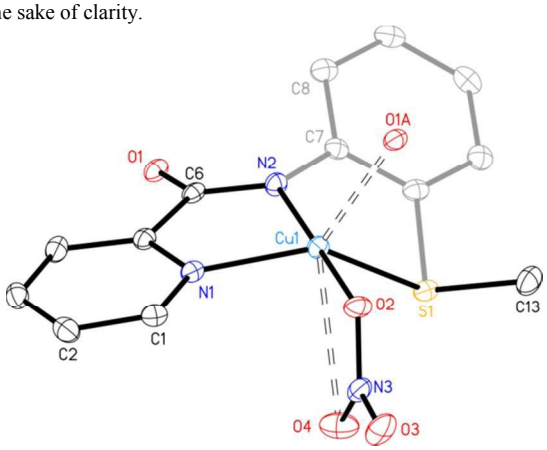

Fig 4. Thermal ellipsoid (probability level 50%) plot of [(L1)Cu(NO$_3$)]$_n$, **5** with the atom labeling scheme. H atoms are omitted for the sake of clarity.

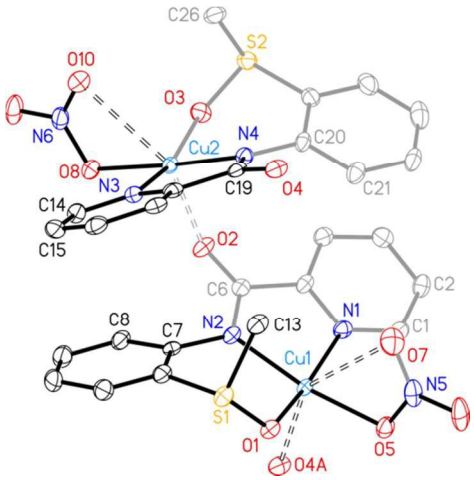

Fig 5. Thermal ellipsoid (probability level 50%) plot of [(L1^{SO})Cu(NO$_3$)]$_n$, **6** with the atom labeling scheme. H atoms are omitted for the sake of clarity.

Table 2. Selected Bond Distances (Å) and angles (°) for Complexes **2** and **4-6**

	[(L1^{SO})Cu(CH$_3$CN)](ClO$_4$), **2**		
Cu(1)-N(1)	2.0035(18)	Cu(1)-N(2)	1.9625(17)
Cu(1)-N(3)	1.9812(19)	Cu(1)-O(1)#1	2.2292(15)
Cu(1)-O(2)	1.9948(15)	Cu(1)-O(3)	3.0639(18)
N(1)-Cu(1)-N(2)	82.24(7)	N(1)-Cu(1)-N(3)	94.75(7)
N(1)-Cu1-O(1)#1	112.97(6)	N(1)-Cu(1)-O(2)	155.76(7)
N(2)-Cu(1)-N(3)	175.46(8)	N(2)-Cu1-O(1)#1	92.30(7)
N(2)-Cu(1)-O(2)	93.96(7)	N(3)-Cu1-O(1)#1	92.00(7)
N(3)-Cu(1)-O(2)	87.39(7)	O(1)-Cu(1)-O(2)	91.03(6)
	[(L1^{SO})Cu(ONO)], **4**		
Cu(1)-N(1)	1.998(2)	Cu(1)-N(2)	1.986(2)

Cu(1)-O(1)#1	2.260(2)	Cu(1)-O(2)	1.9752(19)
Cu(1)-O(3)	2.668(2)	Cu(1)-O(4)	1.976(2)
N(1)-Cu(1)-N(2)	81.95(9)	N(1)-Cu(1)-O(4)	93.15(9)
N(1)-Cu(1)-O(2)	167.42(9)	N(2)-Cu(1)-O(4)	169.93(10)
N(2)-Cu(1)-O(2)	93.75(9)	O(2)-Cu(1)-O(4)	89.19(8)
O(1)#1-Cu(1)-O(3)	143.51(8)	O(3)-N(3)-O(4)	114.6(2)
[(L1)Cu(NO$_3$)], **5**			
Cu(1)-N(1)	2.0156(14)	Cu(1)-N(2)	1.9378(14)
Cu(1)-S(1)	2.4546(4)	Cu(1)-O(2)	1.9411(12)
Cu(1)-O(1)#1	2.1789(11)	Cu(1)-O(4)	2.8369(14)
N(1)-Cu(1)-N(2)	81.93(6)	N(1)-Cu(1)-S(1)	134.57(4)
N(1)-Cu(1)-O(2)	96.81(5)	N(1)-Cu(1)-O(1)	129.81(5)
N(2)-Cu(1)-S(1)	80.26(4)	N(2)-Cu(1)-O(2)	177.71(6)
N(2)-Cu(1)-O(1)#1	93.28(5)	S(1)-Cu(1)-O(2)	101.96(4)
S(1)-Cu(1)-O(1)#1	92.74(3)	O(2)-Cu1-O(1)#1	86.05(5)
[(L1^{SO})Cu(NO$_3$)], **6**			
Cu(1)-N(1)	1.989(5)	Cu(2)-N(3)	1.986(5)
Cu(1)-N(2)	1.977(5)	Cu(2)-N(4)	1.976(5)
Cu(1)-O(1)	1.963(4)	Cu(2)-O(2)	2.222(4)
Cu(1)-O(4)#1	2.232(4)	Cu(2)-O(3)	1.973(5)
Cu(1)-O(5)	1.997(4)	Cu(2)-O(8)	1.985(4)
Cu(1)-O(7)	2.679(5)	Cu(2)-O(10)	2.687(5)
N(1)-Cu(1)-N(2)	82.7(2)	N(3)-Cu(2)-N(4)	82.6(2)
N(1)-Cu(1)-O(1)	167.4(2)	N(3)-Cu(2)-O(2)	106.90(19)
N(1)-Cu(1)-O(4)#1	100.46(19)	N(3)-Cu(2)-O(3)	163.45(19)
N(1)-Cu(1)-O(5)	93.33(19)	N(3)-Cu(2)-O(8)	93.6(2)
N(2)-Cu(1)-O(1)	94.25(19)	N(4)-Cu(2)-O(2)	95.26(18)
N(2)-Cu1-O(4)#1	98.13(18)	N(4)-Cu(2)-O(3)	94.9(2)
N(2)-Cu(1)-O(5)	170.2(2)	N(4)-Cu(2)-O(8)	174.1(2)
O(1)-Cu1-O(4)#1	92.09(17)	O(2)-Cu(2)-O(3)	89.59(18)
O(1)-Cu(1)-O(5)	87.74(18)	O(2)-Cu(2)-O(8)	90.11(17)
O(4)-Cu(1)-O(5)	91.34(17)	O(3)-Cu(2)-O(8)	87.59(18)

Symmetry code : #1 = -x+1,y+1/2,-z+1 for **2**; = x+1/2,-y+1/2,-z for **4**; = x-1/2,-y+1/2,-z+1 for **5**; = x+1, y, z for **6**.

Spectroscopic properties

Electronic spectra and Hydroxylase Activity

The plausible mechanism for the catalytic C-H bond hydroxylation in presence of molecular O_2 by the enzymes PHM and DβM is reported (Supporting Information).[2b] First, O_2 binds to Cu_M(I) of the reduced enzyme. The Cu^I transfers one electron to O_2, therby form a copper(II)-superoxo, $Cu_M(II)\text{-}O_2^{\bullet-}$, intermediate which is then further reduced to copper(II)-peroxo, $CuM(II)\text{-}O_2^{2-}$ or a copper(II)-hydroperoxo, Cu_M(II)-OOH species. Finally a highly reduced copper(II)-oxo radical, $CuM\text{-}O^{\bullet-}$ is formed via the reductive cleavage of Cu_M(II)-OOH species that attacks to the substrate radical, formed after hydrogen abstraction from the substrate, and produce the hydroxylated product. According to the proposed mechanism,[2b] to study the H_2O_2 reactivity of a Cu^{II} model is then a step ahead to study the O_2 reactivity of a Cu^I model complex. The intermediates such as $Cu(I)\text{-}O_2$, $Cu(II)\text{-}O_2^{\bullet-}$ or Cu(II)-OOH and $CuM\text{-}O^{\bullet-}$ are usually highly unstable at room temperature, however, detectable using UV-Vis spectroscopy[11h,11k,12] at low temperature or with the aid of resonance Raman spectra using ^{18}O isotope labeled H_2O_2.[11d] It is then expected that in absence of organic substarte and at room temperature, the Cu^{II} model complexes may undergo ligand oxidation to produce stable products such as sulfur oxidized sulfoxide or sulfone. Choice of protic solvent such as CH_3OH to study the H_2O_2 reactivity is prefered that may serve as proton donor or acceptor during the course of the oxidation reaction.

The electronic absorption spectra of Cu^{II} complexes (**1**-**7**) and of the ligands (HL1, HL1^{SO} and HL1^{SO2}) are measured in solvents such as CH_3OH and CH_3CN. Spectral data are tabulated in Table 3. The electronic spectra of complexes **1**-**7** display weak broad absorption bands in the range 610 nm -690 nm owing to the spin forbidden d-d transition ($\varepsilon < 200\ M^{-1}\ cm^{-1}$). Comparison of this d-d band between the pair of complexes with thioether-S ligated and corresponding sulfoxide-O ligated complexes reveals red shifting (red shifting for **1**→**2** = 59 nm, **3**→**4** = 57 nm and **5**→**6** = 51 nm) for the sulfoxide-O ligated complexes. Further oxidation of sulfoxide (-SO) moiety of **6** to sulfone ($-SO_2$) of **7** also red shifts the lower energy band from 668 nm (**6**) to 692 nm (**7**). In complexes **1**, **3** and **5** the three donors of ligand L1 makes two five membered rings with the central Cu^{II} ion whereas in case of the corresponding sulfoxide ligand, L1^{SO} or L1^{SO2}, one five and a six membered ring formed due to the sulfoxide-O coordination to Cu^{II}. Owing to this expansion of chelate ring size[23] and change of thioether-S to sulfoxide-O donor, the d-d transition for **2**, **4**, **6** and **7** are red shifted. In 300 nm region complex **5** displays three overlapped bands at 296 nm, 308 nm and 330 nm like observed before in the spectrum of **1** and **3** where parent L1 is coordinated to Cu^{II} via its thioether-S donor atom. However, for the corresponding sulfoxide-O ligated complexes a single band, blue shifted than 330 nm, is observed such as for **2** = 324 nm, **4** =320 nm, **6** =324 nm and for **7** =300 nm. The band profile (three overlapped absorption bands versus a single band) correspond to the electronic transition at ~300 nm depends on the type of ligand donor atoms (thioether-S versus sulfoxide/sulfone-O) and of LMCT (ligand to metal charge transfer transition) in origin.[14] The highest energy transitions observed at ~248 nm-260 nm for the complexes **1**-**7** is due to the π-π* transition. Appreciable red shifting (~50 nm-60 nm) of the lowest energy band of the sulfoxide-O ligated complexes compared to that of their precursor thioether-S ligated complexes allows us to monitor this aryl-thioether-S oxidation using UV-Vis spectroscopy. To check whether or not the thioether-S oxidation is stoichiometric, we have titrated the CH_3CN solution of **1** (CH_3CN chosen in this case as the product **2** has Cu^{II} coordinated CH_3CN, see Scheme 1) or the CH_3OH solution of **5** with a solution of equivalent amount of H_2O_2 in respective solvents. The UV-Vis spectral changes of **1** and **5** takes place with the progressive addition of H_2O_2 has been shown in Fig. 6 and Fig. 7 respectively. The isosbestic points at 600 nm, 518 nm, 350 nm, 323 nm and 268 nm shown in Fig. 6 clearly reveals the clean transformation of **1**→**2**. The 573 nm peak of the blue colored CH_3CN solution of **1** splitted into two peaks, one at 650 nm and other at 455 nm those correspond to the peaks found for authentic

isolated complex **2** in CH_3CN. Similar stoichiometric conversion of **5**→**6** has been monitored in CH_3OH for which the isosbestic points found are at 709 nm, 478 nm, 389 nm and 267 nm (Fig. 7).

Table 3. Electronic absorption spectral data of **1**-**7** and of ligands HL1, $HL1^{SO}$ and $HL1^{SO2}$, data of **1** and **6** are taken from Ref. 14.

Compound/Solvent	λ_{max}, nm (ε, M^{-1} cm^{-1})
1 : CH_3OH	258 (13000), 285 (7915), 297 (8050), 310 sh (7810), 330 sh (6940),455 sh (110), 626 (150)
: CH_3CN	260 (12740), 300 (8160), 312 sh (7630), 330 sh (6450), 573 (190)
2 : CH_3OH	257 (13360), 324 (7710), 448 (232), 685 (118)
: CH_3CN	260 (12060), 324 (6870), 455 (204), 650 (114)
3 : CH_3OH	257 (14480), 298 (8540), 310 (8280), 327 sh (7730), 613 (157)
4 : CH_3OH	257 (11 190), 320 (6 185), 670 (110)
5 : CH_3OH	257 (14 240), 296 (8775), 308 (8 370), 330 (7500), 455 (125), 627 (154)
6 : CH_3OH	257 (10 580), 324 (5840), 438 (197), 668 (91)
7 : CH_3OH	248 (7575), 300 (4720), 692 (81)
HL1: CH3OH	263 (8070), 286 (7130)
$\mathbf{HL1^{SO}}$: CH_3OH	205 (8570), 216 sh (6090), 268 (2760), 290 (2220)
$\mathbf{HL1^{SO2}}$: CH_3OH	205 (18630), 216 sh (13160), 270 (5600), 290 (4700)

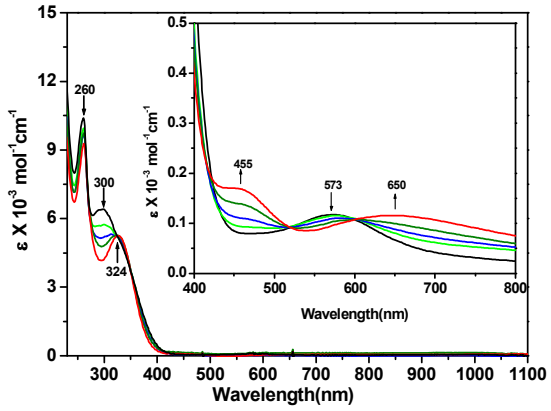

Fig. 6: Electronic absorption spectral changes during transformation of **1** (black trace)→ **2** (red trace) when titrating a CH_3CN solution of **1** (10 mL, $1x10^{-3}$ M) with a CH_3CN solution of H_2O_2 (1 µl of 30% H_2O_2 dissolved in 100 µl CH_3CN). Each scan is taken, after addition of 25 µl of H_2O_2 solution.

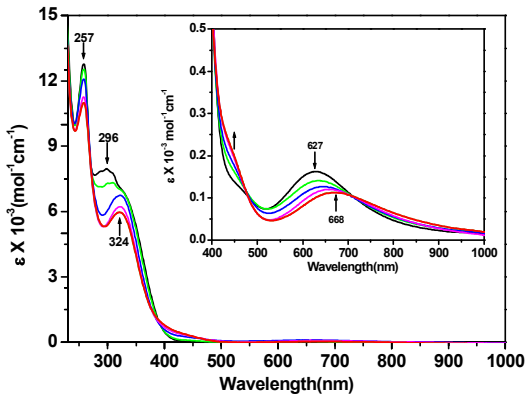

Fig. 7: Electronic absorption spectral changes during transformation of **5** (black trace)→ **6** (red trace) when titrating a CH_3OH solution of **5** (10 mL, $1x10^{-3}$ M) with a CH_3OH solution of H_2O_2 (1 µl of 30% H_2O_2 dissolved in 100 µl CH_3OH). Each scan is taken, after addition of 25 µl of H_2O_2 solution.

Interestingly, when a CH_3OH solution of **3** is treated with two equivalent of H_2O_2 the lower energy d-d band at 613 nm of **3** is red shifted to 668 nm that correspond to that of **6**. This stoichiometric conversion of **3** + $2H_2O_2$ →**6**, lacks clean isosbestic points in its absorption spectra as shown in Fig. 8 that hints formation of a mixture of complexes like **4**, **5** and **6** in various proportion rather than forming solely **6**. H_2O_2 oxidizes the thioether-S of Cu^{II} coordinated ligand L1→$L1^{SO}$ and NO_2^- →NO_3^- both and consequently transforms **3**→**6**. To justify whether there is any preference of oxidation of thioether-S→thioether-SO *versus* NO_2^-→NO_3^-, we have investigated the electronic spectral changes occur upon addition of just one equivalent of H_2O_2 to the CH_3OH solution of **3** (Supporting Information). The final trace of the electronic spectrum after complete addition of one equivalent H_2O_2 clearly demonstrates the formation of **4**, **5** and **6**, as is evident from the occurrence of broad absorption band centered at 627 nm, corresponds to that of **5** and at ~ 670 nm corresponds to that of **4** and **6** (Table 3). Thus the oxidation of both thioether-S and the NO_2^- ion, coordinated to Cu^{II}, are equally probable. In fact, addition of stoichiometric H_2O_2 to a CH_3OH solution of **4**, where thioether-S is already in thioether-SO form, oxidizes the Cu^{II} bound NO_2^- to NO_3^- and produces stoichiometric **6** that has been monitored by UV-Vis spectroscopy as shown in Fig. 9. The isosbestic points observed at 260 nm, 300 nm and 366 nm indicates a clean conversion of **4**→**6**. There are two possible pathways for Cu^{II} coordinated ligand oxidations. One pathway is that the oxidant, H_2O_2 may first binds to the Cu^{II} to form the transient Cu^{II}-OOH species[11k] that finally lead to Cu^{II} bound ligand thioether-S and/or NO_2^- oxidation. The second possibility is that the H_2O_2 present in the second coordination sphere and attack to the electrophilic centers such as thioether-S or N atom of NO_2^- ion. We do not investigate the UV-Vis spectral changes takes place at low temperature after addition of H_2O_2 to a solution of samples under investigation that may enlighten to the mechanistic pathways, however, no de-coordination of the parent thioether-S ligand is evident from the UV-Vis absorption spectral changes occurs upon addition of H_2O_2 to a solution of **1** and **3**-**5** at room temperature. Strong support that no de-coordination of L1 occurs are: the lower energy d-d band, characteristic to the ligand-Cu^{II} system, is retained in all traces as shown in Fig. 6-10 and much higher extinction coefficient, ε, value of ~270 nm band (~8,000-14,000 $M^{-1}cm^{-1}$) for **1**-**7** than the ε values of the free ligands $L1^{SO}$ or $L1^{SO2}$ (Table 3).

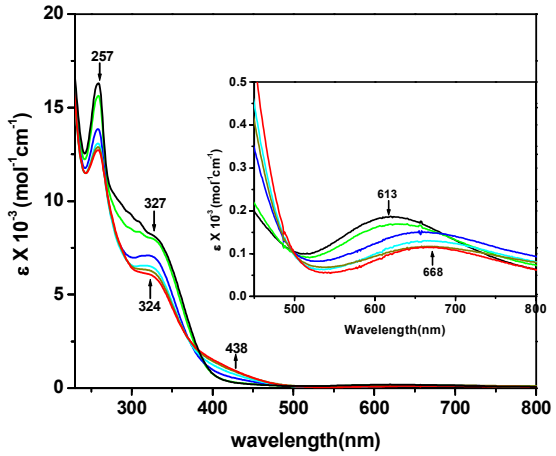

Fig. 8: Electronic absorption spectral changes during transformation of **3** (black trace)→ **6** (red trace) when titrating a CH_3OH solution of **3** (10 mL, $1x10^{-3}$ M) with a CH_3OH solution of $2H_2O_2$ (2 µl of 30% H_2O_2 dissolved in 100 µl CH_3OH). Each scan is taken, after addition of 20 µl of H_2O_2 solution.

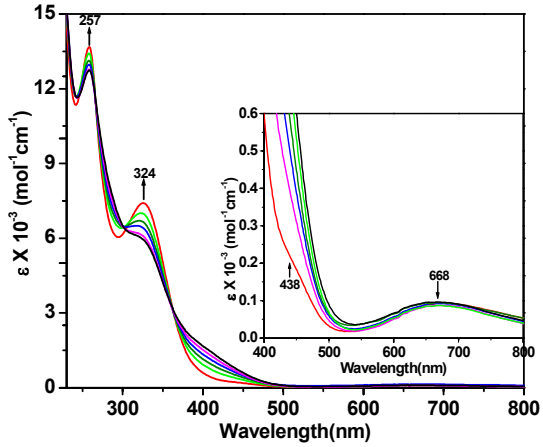

Fig. 9: Electronic absorption spectral changes during transformation of **4** (black trace)→ **6** (red trace) when titrating a CH_3OH solution of **4** (10 mL, $1x10^{-3}$ M) with a CH_3OH solution of H_2O_2 (1 µl of 30% H_2O_2 dissolved in 100 µl CH_3OH). Each scan is taken, after addition of 20 µl of H_2O_2 solution.

To test whether further oxidation of sulfoxide (-SO(CH_3)) to sulfone (-SO_2(CH_3)) is possible, the CH_3OH solution of NO_3^- bound Cu^{II} complex of $L1^{SO}$, **6** is treated with an equivalent of H_2O_2 and the UV-Vis spectral changes were recorded as shown in Fig. 10. Red shifting of absorption band from 668 nm to 692 nm and blue shifting of the bands from 324 nm and 257 nm to 300 nm and 248 nm respectively is evident. The absorption maxima such as 692 nm, 300 nm and 248 nm, observed in the final trace (red trace) after complete addition of H_2O_2, are same to those of NO_3^- bound Cu^{II} complex of $L1^{SO2}$, **7** that indicates **6→7** conversion. In addition, the isosbestic points observed at 398 nm, 366 nm, 315 nm, 268 nm and 237 nm reveals that **6→7** conversion is clean and no other intermediate product is formed during the course of the transformation. No observation of formation of **7** is evident from the UV-Vis spectral study carried out for conversions of **3-5→6**. Therefore, **6→7** conversion (Fig. 10) proves that H_2O_2 oxidation of thioether-SO → thioether-SO_2 is less facile than the thioether-S → thioether-SO (**3→6**, **5→6** conversion) and NO_2^-→NO_3^- (**4→6** conversion) conversions. Therefore, the oxidation reaction of Cu^{II} coordinated ligand thioether-S or thioether-SO and/or NO_2^- ensues according to Scheme 3 as shown below. The lowest energy λ_{max} values of the corresponding complexes (see Scheme 3) reveal that oxidation of the Cu^{II} coordinated thioether-S → thioether-SO or O coordinated thioether-SO→ thioether-SO_2 red shifts the lowest energy band ~50 nm and 26 nm respectively whereas the oxidation of NO_2^- → NO_3^- hardly shifts the band position.

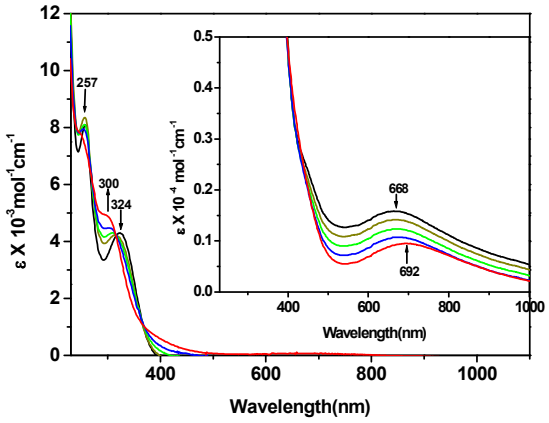

Fig. 10: Electronic absorption spectral changes during transformation of **6** (black trace)→ **7** (red trace) when titrating a CH_3OH solution of **6** (10 mL, $1x10^{-3}$ M) with a CH_3OH solution of H_2O_2 (1 µl of 30% H_2O_2 dissolved in 100 µl CH_3OH). Each scan is taken, after addition of 25 µl of H_2O_2 solution.

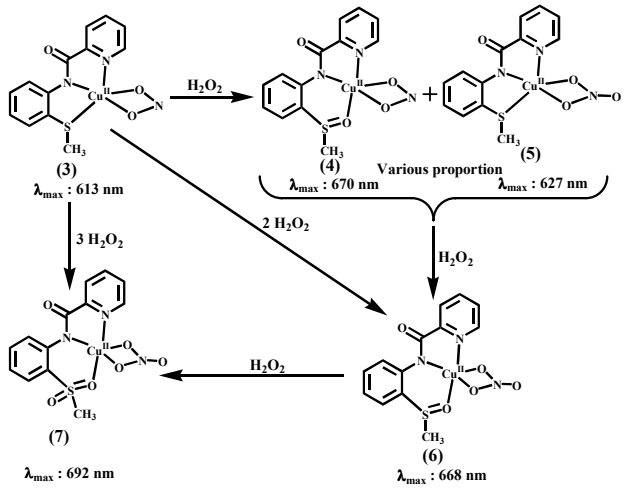

Scheme 3: Copper mediated thioether-S, thioether-SO and NO_2^- oxidation using H_2O_2 oxidant

Redox chemistry

To investigate, how the Cu^{II} chelated ligands are susceptible to oxidations and stabilize the Cu^{II} state, we have recorded the cyclic voltammograms (CV) of the complexes in CH_3CN. The

CV trace of a representative complex **5** has been shown in Fig. 11 and the potential values for other complexes are summarized in Table 4. CV of **5** features two reductive responses, one irreversible response at E_{pc} = -0.08 V and other, a quasi-reversible response at $E_{1/2}$ = -0.46 V (E_{pc} = -0.51 V, E_{pa} = -0.42 V, ΔE_p = 90 mV) correspond to the $Cu^{II} \rightarrow Cu^{I}$ and $Cu^{I} \rightarrow Cu^{0}$ reduction respectively. The i_{pa}/i_{pc} ratio of the response at $E_{1/2}$ = -0.46 V is much less than unity that clearly indicates the re-oxidation of Cu^0 species to Cu^I is partial. The full transformation occurs beyond the stripping potential at E_s = -0.24 V. CV scan towards positive potential displays one irreversible oxidative response at E_{pa} = + 1.39 V like observed for the L1 ligated complexes, **1** and **3**, which are at +1.40 V and +1.38 V respectively.[14] This response is due to the ligand centered oxidation and not due to the $Cu^{II} \rightarrow Cu^{III}$ conversion, proved from the CV measurement of a mixture of deprotonated $L1^-$ in presence of equivalent amount of Zn^{2+} salt, that also shows an oxidation wave at E_{pa} = + 1.34 V (Supporting Information). There are two susceptible parts on the ligand frame to get oxidized, one is the aromatic phenyl ring adjacent to the amide functional group and other is the thioether sulfur atom. Amide ligand cation radical[24] as well as sulfur cation radical[25] complexes are known. Most interestingly, the CV scans of the Cu^{II} complexes ligated to $L1^{SO}$ (**2**, **4**, **6**) or $L1^{SO2}$ (**7**) does not display this oxidation wave up to + 1.6 V, checked (Supporting Information). As the ligand L1 is already in the sulfur oxidized forms ($L1^{SO/SO2}$) the oxidative response at E_{pa} ~ +1.40 V possibly is absent. This observation apparently indicates that potential observed for L1 ligated complexes at ~+1.40 V is due sulfur centered oxidation of ligand L1. However, as both the thioether sulfur and the amide functional group are in *ortho* positions to the same phenyl ring, that makes the system delocalized, the exact location of oxidation can't be identified unambiguously.

Scrutiny of the potential values, shown in Table 4, indicates that the nitrate ligated complexes **5**, **6** and **7** displays much more anodic Cu^{II}/Cu^{I} reduction potentials, at -0.08 V, -0.06 V and +0.12 V respectively, than the nitrite bound complexes **3** and **4** those are at -0.41 V and -0.39 V respectively. This drastic potential shift between the set of complexes is unexpected as a similar asymmetric coordination mode of binding for both nitrate and nitrite anion to Cu^{II} is observed (Table 2). Also close lower energy λ_{max} values (613 nm and 668 nm of **3** and **4** versus 627 nm and 670 nm of **5** and **6**, Table 3) and a similar EPR spectral profile and g values (g_{II} = 2.20, $g_{\perp}$ = 1.99, A_{II} = 175 G; see Supporting Information) are observed for both nitrate and nitrite bound complexes in CH_3CN. This clearly hints that not the CH_3CN solvent but the excess ClO_4^-, used as supporting electrolyte, $(n\text{-Bu})_4NClO_4$, during CV measurement, replaces the NO_3^- of **5**-**7**. After addition of 40 equivalents of NO_3^- to the same solution and repeated CV scan shows a cathodic shift of this potential to -0.26 V, -0.44 V and –0.27 V for 5-7 respectively (Supporting Information) due to NO_3^- re-coordination by replacing ClO_4^-. No such dislacement of NO_2^- by ClO_4^- of supporting electrolyte is observed for **3** and **4** during CV measurement.

The redox properties of the enzyme bound Cu in DβM is reported by Ljones et al and others.[26] The reduction potential obtained are +385±15 mV and +360±15 mV from anaerobic and aerobic redox titration respectively *vs* SCE reference electrode. The high positive reduction potential for Cu^{II}/Cu^{I} couple is essential for efficient enzymatic activity. The Cu_M site maintain distorted tetrahedral geometry during catalytic activity. As the reduced Cu_M^I prefers a tetrahedral geometry and the donors like $(His\text{-}N)_2S_{Met}O_w$ surrounding metal ion are neutral the $Cu^{II} \rightarrow Cu^{I}$ reduction is highly favorable and has high positive value, unlike **1** where the Cu^{II} has a square pyramidal geometry with a strong σ-donor amidato N^- coordination that favors Cu^{II} state stabilization and hence more cathodic value like +30 mV than the Cu_M of DβM.

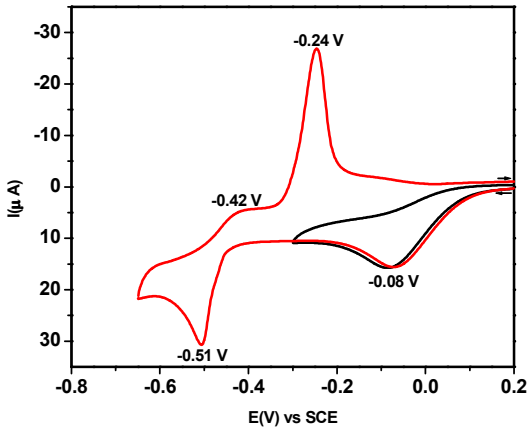

Fig. 11. Cyclic voltammograms of **5** in CH_3CN containing 0.1 M $[(n\text{-}Bu)_4N]ClO_4$ as a supporting electrolyte at 298 K at a platinum working electrode at a scan rate of 50 mV s^{-1} using *SCE* as reference electrode.

Table 4. Electrochemical data for the complexes **1**-**7** (measured in CH_3CN solution)

Complex	Reductive Response		Oxidative Response	Ref.
	E_{pc}, V	$E_{1/2}$[a], V (ΔEp[b], mV) E_s[c]	E_{pa}, V	
1	+0.03,[d] -0.33[e]	-0.50 (130) -0.33	+1.40	14
2	-0.02,[d] -0.19[e]	-0.44 (90) -0.32	-	This work
3	-0.41	-0.51 (110) -0.33 -0.62 (80) -0.28	+1.38	14
4	-0.39	-0.55(60) -0.35	-	This work
5	-0.08	-0.46 (90) -0.24	+1.39	This work
6	-0.06	-0.47 (130) -0.21	-	This work
7	+0.12	-0.50 (130) -0.30	-	This work
HL1			+1.45	14
NaL1+Zn^{2+}			+1.34	14

Potentials are *vs.* SCE (Fc/Fc^+ = + 0.43V), scan rate 50 mV/s, supporting electrolyte: $n\text{-}Bu_4NClO_4$ (0.1 M). [a]$E_{1/2} = (E_{pc} + E_{pa})/2$, [b]$\Delta E_p = E_{pa} - E_{pc}$. [c]$E_s$ is stripping potential of $Cu^0 \rightarrow Cu^{2+}$ oxidation, [d]solvent bound complex, [e]broad shoulder, may be due to ClO_4^- coordinated species, [$(L1/L1^{SO})Cu(ClO_4)$].

Conclusions

Cu^{II} complexes with supporting tridentate N_2S donor ligands have been synthesized and characterized. The oxidative activity of Cu^{II} complexes, where Cu is coordinated to $N_2S_{thioether}$ donor ligand,

HL1 and NO_2^-, have been investigated using oxidants such as *m*-CPBA, H_2O_2 and molecular O_2. Absorption spectral changes upon H_2O_2 titration of complex's solutions reveals that $L1 \rightarrow L1^{SO}$ and $NO_2^- \rightarrow NO_3^-$ oxidation are equally probable. It has also been found that $L1^{SO} \rightarrow L1^{SO2}$ oxidation is less preferred than both $L1 \rightarrow L1^{SO}$ and $NO_2^- \rightarrow NO_3^-$ oxidation. Absence of oxidative response up to +1.6 V reveals coordination of thioether-S oxidized ligands, $L1^{SO}$ or $L1^{SO2}$ to Cu^{II}. To the best of our knowledge complexes **2**, **4** and **6** are the first structurally characterized copper complexes where aromatic thioether-S oxidation is evident. Easy oxidation of aromatic thioether-S, thioether-SO and NO_2^- in the present work may enrich the data base regarding why the Cu_M site of hydroxylases choose non planar aliphatic thioether, Met-S, coordination for substrate hydroxylation with no prevalence of Met-S oxidation to sulfoxide or sulfone. Moving from thioether-S to sulfoxide-O donor red shifted the lower energy d-d band ~60 nm. Further red shift of the d-d band, ~25 nm, is observed going from thioether-SO to thioether-SO_2 conversion. The amide-N donor highly stabilized the Cu^{II} state of the present complexes.

Acknowledgement

Financial support from the Department of Science and Technology (DST), Govt. of India (SR/S1/IC-35/2007) is gratefully acknowledged. R. C. Maji acknowledged the support of UGC for fellowship. We sincerely acknowledge the AvH Foundation, Germany, for the equipment donation grant to procure the CHI-1120A spectroelectrochemical analyzer. We thank the Advanced Light Source, Lawrence Berkeley Lab, for use of beamline 11.3.1 for X-ray data collection. The Advanced Light Source is supported by the Director, Office of Science, Office of Basic Energy Sciences, of the U.S. Department of Energy under Contract No. DE-AC02-05CH11231.

Notes and references

[a]*Department of Chemistry,National Institute of Technology Durgapur, Mahatma Gandhi Avenue, Durgapur 713209, West Bengal, India. Tel:+91(0343)275-5475; E-mail: apurba.patra.nitdgp@gmail.com*
[b]*Department of Chemistry, Indian Institute of Technology Kanpur, Kanpur 208016, India.*
[c]*Department of Chemistry, University of California, Davis, CA 95616 (USA)*

† Electronic Supplementary Information (ESI) available: FTIR spectrum of **4**, **5** and **6** as Fig. S1-S3, ^{1}H NMR spectrum of $L1^{SO}$ (Fig. S4), Mass spectrum of $L1^{SO}$ and $L1^{SO2}$ (Fig. S5-S6), CV of HL1, **5**, **6** and **2** (Fig. S7-S10), Electronic absorption spectral changes $[(L1)Cu^{II}(ONO)]_n$ (**3**) +1 H_2O_2 (Fig, S11), and 3-D polymeric view of **6** (Fig. S12), Mechanism of reference 2(b) (Fig. S13), Cyclic voltammogram of **5**, **6**, **7** and in presence of **5** or **6** or **7** + 40 equiv $NaNO_3$ (Fig. 14-S16), X-band EPR spectra of **3** or **5** in MeCN-toluene at 298 K and 77 K (Fig. S17-S18) and X-ray crystallographic data of **4**-**6** and **2** as CIF file (CCDC reference numbers for **4**, **5**, **6** and **2** as 1402244-1402247). This material is available free of charge via the internet See DOI: xx.xxxx/b000000x/

1 (a) S. T. Prigge, A. S. Kolhekar, B. A. Eipper, R. E. Mains and L. M. Amzel, *Science*, 1997, **278**, 1300-1305; (b) X, Siebert, B. A. Eipper, R. E. Mains, S. T. Prigge, N. J. Blackburn, L. M. Amzel, *Biophysical journal,* 2005, **89**, 3312-3319; (c) E. I. Solomon, D. E. Heppner, E. M. Johnston, J. W. Ginsbach, J. Cirera, M. Qayyum, M. T. Kieber-Emmons, C. H. Kjaergaard, R. G. Hadt and L. Tian, *Chem. Rev.*, 2014, **114**, 3569-3853.

2 (a) N. J. Blackburn, M. Concannon, S. K. Shahiyan, F. E. Mabbs and D. Collison, *Biochemistry*, 1988, **27**, 6001-6008; (b) J. P. Klinman, *J. Biol. Chem.*, 2006, **281**, 3013-3016.

3 C. R. Hess, M. M. McGuirl, J. P. Klinman, *J. Biol. Chem.*, 2008, **283**, 3042.

4 (a) J. P. Klinman, *Chem. Rev.*, 1996, **96**, 2541-2562; (b) E. A. Lewis and W. B. Tolman, *Chem. Rev.*, 2004, **104**, 1047-1076.

5 D. Bousquet-Moore, R. E. Mains and B. A. Eipper, *J. Neurosci. Res.*, 2010**, 88**, 2535.

6 S. T. Prigge, B. A. Eipper, R. E. Mains and L. M. Amzel, *Science*, 2004, **304**, 864-867.

7 (a) E. E. Chufán, S. T. Prigge, X. Siebert, B. A. Eipper, R. E. Mains and L. M. Amzel, *J. Am. Chem. Soc.,* 2010, **132**, 15565-15572; (b) K. Rudzka, D. M. Moreno, B. Eipper, R. Mains, D. A. Estrin and L. M. Amzel, *J. Biol. Inorg. Chem.*, 2013, **18**, 223.

8 (a) N. J. Blackburn, F. C. Rahmes, M. Ralle and S. Jaron, *J. Biol. Inorg. Chem.*, 2000, **5**, 341; (b) P. Chen and E. I. Solomon, *J. Am. Chem. Soc.,* 2004, **126**, 4991.

9 S. T. Prigge, A. S. Kolhekar, B. A. Eipper, R. E. Mains and L. M. Amzel, *Nat. Struct. Biol.*, 1999, **6**, 976.

10 J. P. Evans, K. Ahn and J. P. Klinman, *J. Biol. Chem.*, 2003, **278**, 49691.

11 (a) K. D. Karlin, M. S. Nasir, B. I. Cohen, R. W. Cruse, S. Kaderli and A. D. Zuberbühler, *J. Am. Chem. Soc.*, 1994, **116,** 1324-1336; (b) G. Alzuet, L. Casella, M. L. Villa, O. Carugo and M. Gullotti, *J. Chem. Soc., Dalton Trans.*, 1997, 4789-4794; (c) E. Pidcock, H. V. Obias, C. X. Zhang, K. D. Karlin and E. I. Solomon, *J. Am. Chem. Soc.*, 1998, **120**, 7841-7847; (d) T. Ohta, T. Tachiyama, K. Yoshizawa, T. Yamabe, T. Uchida and T. Kitagawa, *Inorg. Chem.*, 2000, **39**, 4358-4369; (f) N. W. Aboelella, B. F. Gherman, L. M. R. Hill, J. T. York, N. Holm, V. G. Young, C. J. Cramer and W. B. Tolman, *J. Am. Chem. Soc.*, 2006, **128**, 3445-3458; (g) L. Zhou, D. Powell and K. M. Nicholas, *Inorg. Chem.*, 2006, **45**, 3840-3842; (h) Y. Lee, D-H. Lee, A. A. N. Sarjeant, L. N. Zakharov, A. L. Rheingold and K. D. Karlin, *Inorg. Chem.*, 2006, **45**, 10098-10107; (i) L. Zhou, D. Powell and K. M. Nicholas, *Inorg. Chem.*, 2007, **46**, 7789-7799; (j) D-H. Lee, L. Q. Hatcher, M. A. Vance, R. Sarangi, A. E. Milligan, A. A. N. Sarjeant, C. D. Incarvito, A. L. Rheingold, K. O. Hodgson, B. Hedman, E. I. Solomon and K. D. Karlin, *Inorg. Chem.*, 2007, **46**, 6056-6068; (k) S. Kim, J. Y. Lee, R. E. Cowley, J. W. Ginsbach, M. A. Siegler, E. I. Solomon, K. D. Karlin *J. Am. Chem. Soc.* 2015, **137,** 2796-2799; (l) I. Castillo, V. M. Ugalde-Saldívar, L. A. R. Solano, B. N. S. Eguía, E. Zeglio, E. Nordlander, *Dalton Trans.,* 2012, **41**, 9394-9404; (m) B. N. Sáchez-Equía, M. Flores-Alamo, M. Orio, I. Castillo, *Chem. Commun.*, 2015, **51**, 11134-11137.

12 M. Kodera, T. Kita, I. Miura, N. Nakayama, T. Kawata, K. Kano and S. Hirota, *J. Am. Chem. Soc.,* 2001, **123**, 7715-7716.

13 S. K. Chatterjee, S. Roy, S. K. Barman, R. C. Maji, M. M. Olmstead and A. K. Patra, *Inorg. Chem.*, 2012, **51**, 7625-7635.

14 R. C. Maji, S. K. Barman, S. Roy, S. K. Chatterjee, F. L. Bowles, M. M. Olmstead and A. K. Patra, *Inorg. Chem.*, 2013, **52**, 11084-11095.

15 *Apex 2 v2.1-0*, Bruker AXS, Madison, WI, 2006.

16 G. M. Sheldrick, *Acta Crystallogr., Sect. A,* 1990, **46**, 467.

17 G. M. Sheldrick, *XP*, University of Göttingen, Germany, 1997.

18 K. Nakamoto, *Infrared and Raman Spectra of Inorganic and Coordination Compounds*, *Part B*, Sixth Edn., John Wiley & Sons, Inc., New Jersy, 2006, pp-1874-1877.

19 W. J. Geary, *Coord. Chem. Rev.*, 1971, **7**, 81.

20 A. W. Addison, T. N. Rao, J. Reedijk, J. V. Rijn, G. C. Verschoor, *J. Chem. Soc., Dalton Trans.* 1984, 1349.

21 (a) E. C. M. Ording-Wenker, M. A. Siegler, M. Lutz and E. Bouman, *Inorg. Chem.*, 2013, **52**, 13113-13122; (b) L. S. Higashi, M. Lundeen, E. Hilti and K. Seff, *Inorg. Chem.*, 1977, **16**, 310-313; (c) M. Calligaris, *Coord. Chem. Rev.*, 2004, **248**, 351-375.

22 (a) P. J. Farmer, J. H. Reibenspies, P. A. Lindahl and M. Y. Darensbourgh, *J. Am. Chem. Soc.,* 1993, **115**, 4665–4674; (b) R. M. Buonomo, I. Font, M. J. Maguire, J. H. Reibenspies, T. Tuntulani and M. Y. Darensbourgh, *J. Am. Chem. Soc.,* 1995, **117**, 963–973; (c) C. S. Mullins, C. A. Grapperhaus, B. C. Frye, L. H. Wood, A. J. Hay, R. M. Buchanon and M. S. Mashuta, *Inorg. Chem.*, 2009, **48**, 9974-9976.

23 (a) D. Sanna, C. G. Ágoston, G. Micera, I. Sóvágó, *Polyhedron*, 2001, **20**, 3079-3090; (b) E. A. Ambundo, M-V. Deydier, A. J. Grall, N. Aguera-Vega, L. T. Dressel, T. H. Cooper, M. J. Heeg, L. A. Ochrymowycz, D. B. Rorabacher, *Inorg. Chem.* 1999, **38**, 4233-4242.

24 (a) A. K. Patra, M. Roy and R. Mukherjee, *Inorg. Chem.*, 2000, **39**, 652; (b) A. K. Singh, V. Balamurugan and R. Mukherjee, *Inorg. Chem.*, 2003, **42**, 6497; (c) S. K. Dutta, U. Beckmann, E. Bill, T. Weyhermüller and K. Wieghardt, *Inorg. Chem.*, 2000, **39**, 3355; (d) T. J. Collins, R. D. Powell, C. Slebodnick and E. S. Uffelman, *J. Am. Chem. Soc.*, 1991, **113**, 8419.

25 (a) A. K. Patra, E. Bill, E. Bothe, K. Chlopek, F. Neese, T. Weyhermüller, K. Stobie, M. D. Ward, J. A. McCleverty and K. Wieghardt. *Inorg. Chem*, 2006, **45**, 7877-7890; (b) A. K. Patra, E. Bill, T. Weyhermüller, K. Stobie, Z. Bell, M. D. Ward, J. A. McCleverty and K. Wieghardt. *Inorg. Chem*, 2006, **45**, 6541-6548; (c) D. Dondi, P. Cimino, V. Barone, A. Buttafava, O. Lanzalunga and A. Faucitano, *Tetrahedron Let.*, 2011, **52**, 4097; (d) P. R. Martínez-Alanis, B. N. S. Eguía, V. M. Ugalde-Saldívar, I. Regla, P. Demare, G. Aullón, I. Castillo, *Chem. Eur. J.* 2013, **19**, 6067-6079.

26 (a) T. Ljones, T. Flatmark, T. Skotland, L. Petersson, D. Bäckström, A. Ehrenberg, *FEBS Letters*, 1978, **92**, 81-84; (b) G. A. Walker, H. Kon, W. Lovenberg, *Biochimica et Biophysica Acta,* 1977, **482**, 309-322.

Copper Coordinated Ligand Thioether-S and NO_2^- Oxidation: Relevance to Cu_M Site of Hydroxylases

Ram Chandra Maji[a)], *Anirban Bhandari*[a)], *Ravindra Singh*[b)], *Suprakash Roy*[a)], *Sudip K. Chatterjee*[a)], *Faye L. Bowles*[c)], *Kamran B. Ghiassi*[c], *Milan Maji*[a)], *Marilyn M. Olmstead*[c)], *Apurba K. Patra**[a)]

[a)]Department of Chemistry, National Institute of Technology Durgapur, Mahatma Gandhi Avenue, Durgapur 713 209, India

[b)]Department of Chemistry, Indian Institute of Technology Kanpur, Kanpur 208 016, India

[c)]Department of Chemistry, University of California, Davis, CA 95616 (USA)

Email: apurba.patra.nitdgp@gmail.com

Table of contents

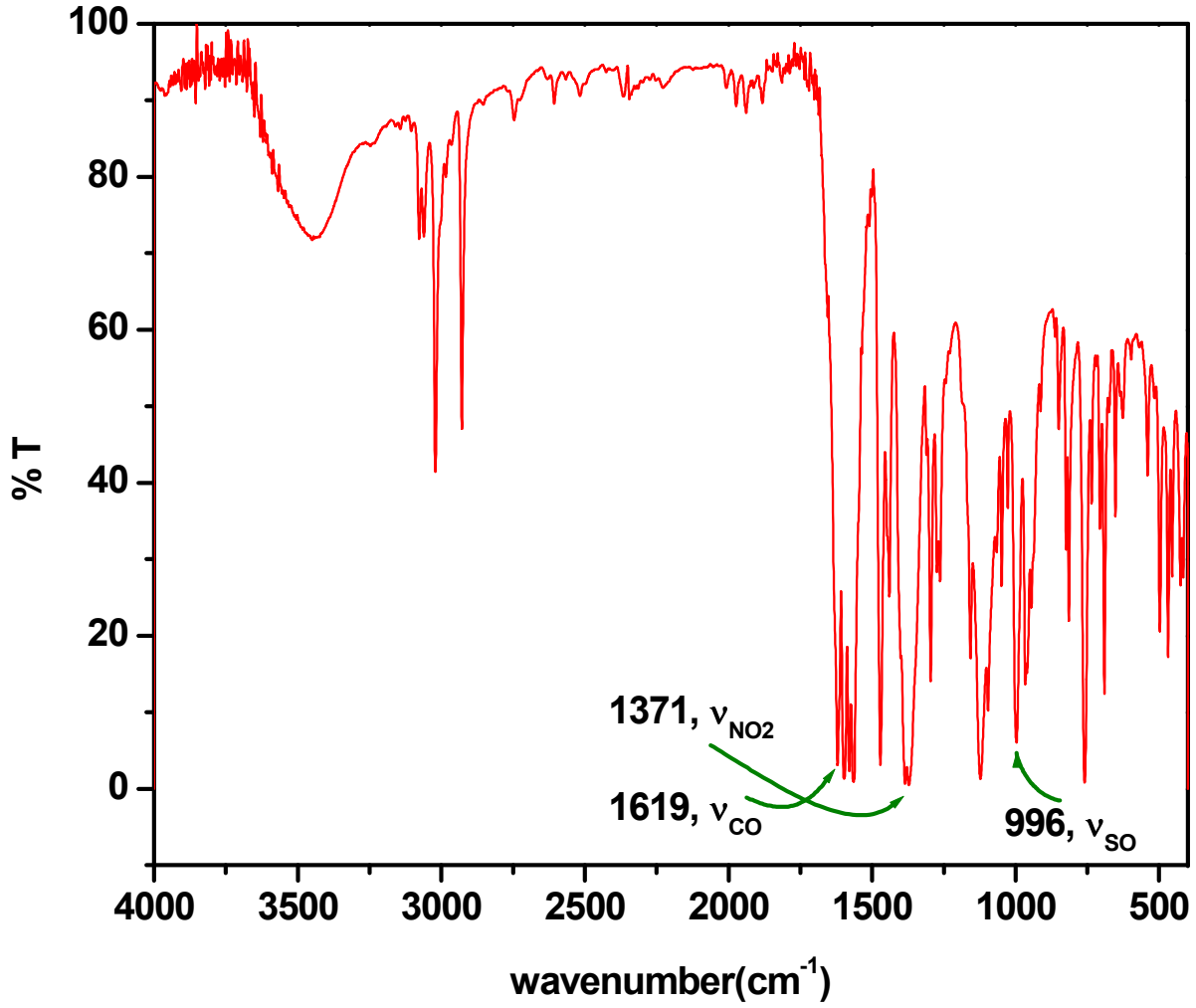

Fig. S1. FTIR spectrum of [(L1^{SO})Cu^{II}(ONO)] (**4**) in KBr disk (400 cm^{-1}-4000 cm^{-1})

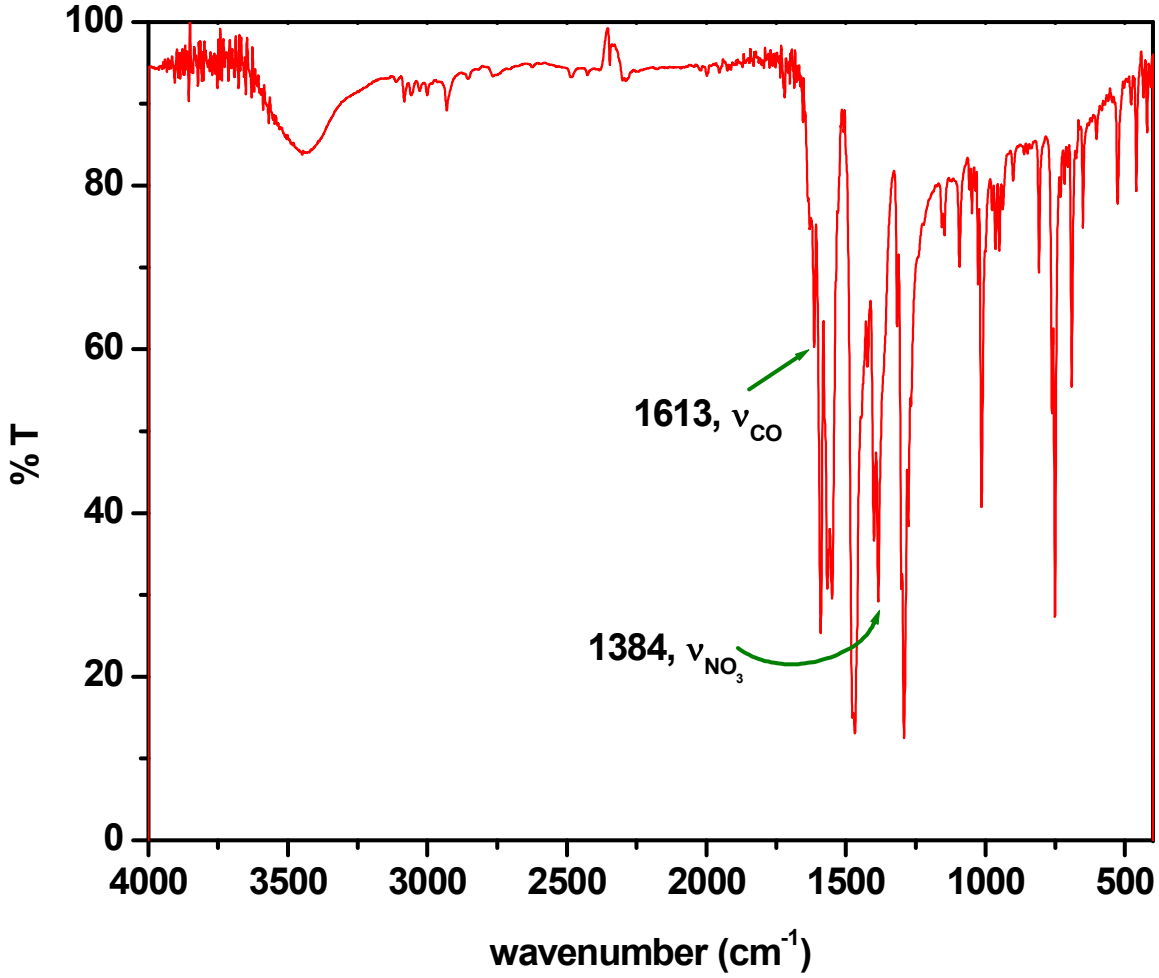

Fig. S2. FTIR spectrum of [(L1)$Cu^{II}(NO_3)$] (**5**) in KBr disk (400 cm^{-1}-4000 cm^{-1})

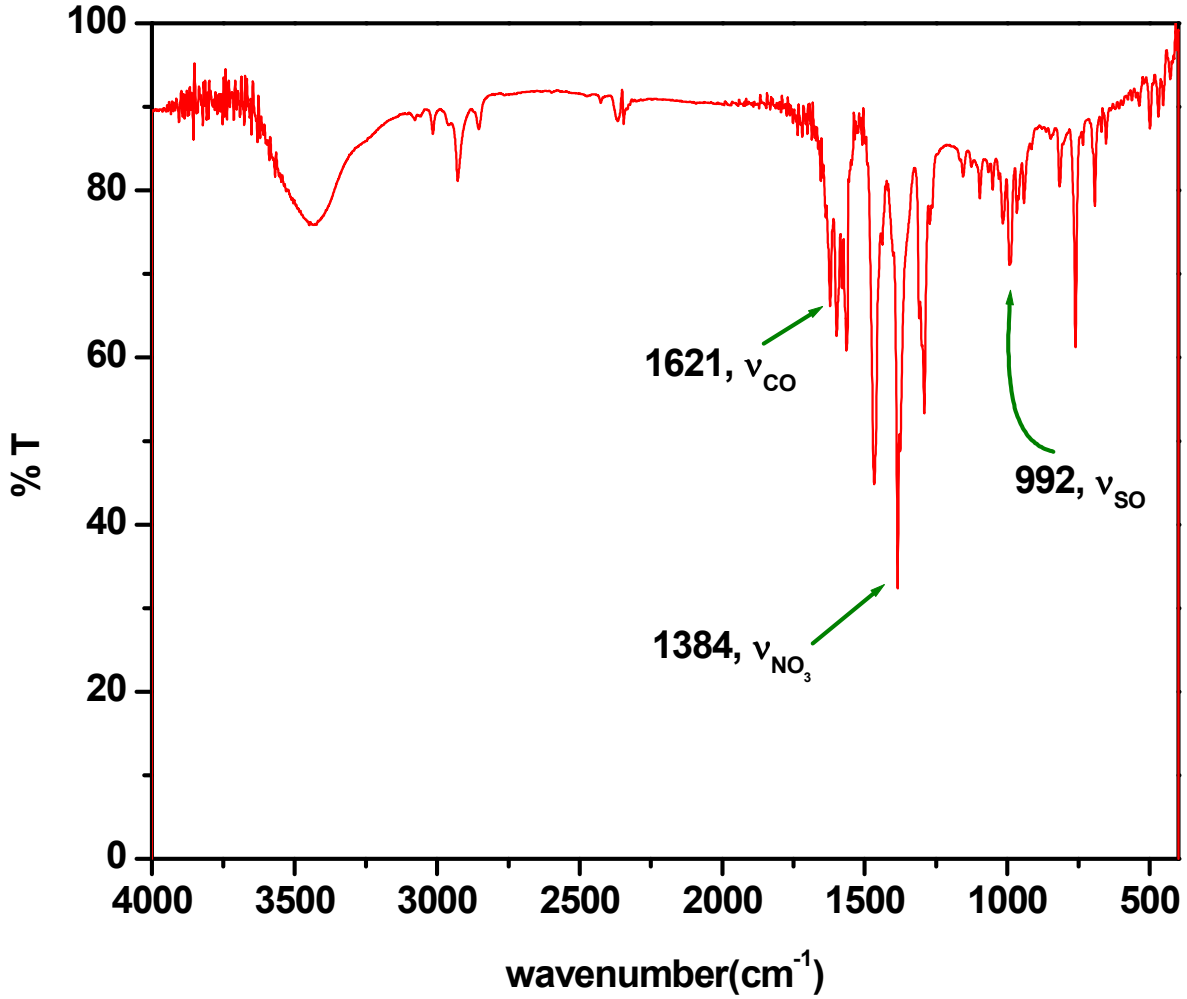

Fig. S3. FTIR spectrum of [(L1^{SO})Cu^{II}(NO$_3$)] (**6**) in KBr disk (400 cm^{-1}-4000 cm^{-1})

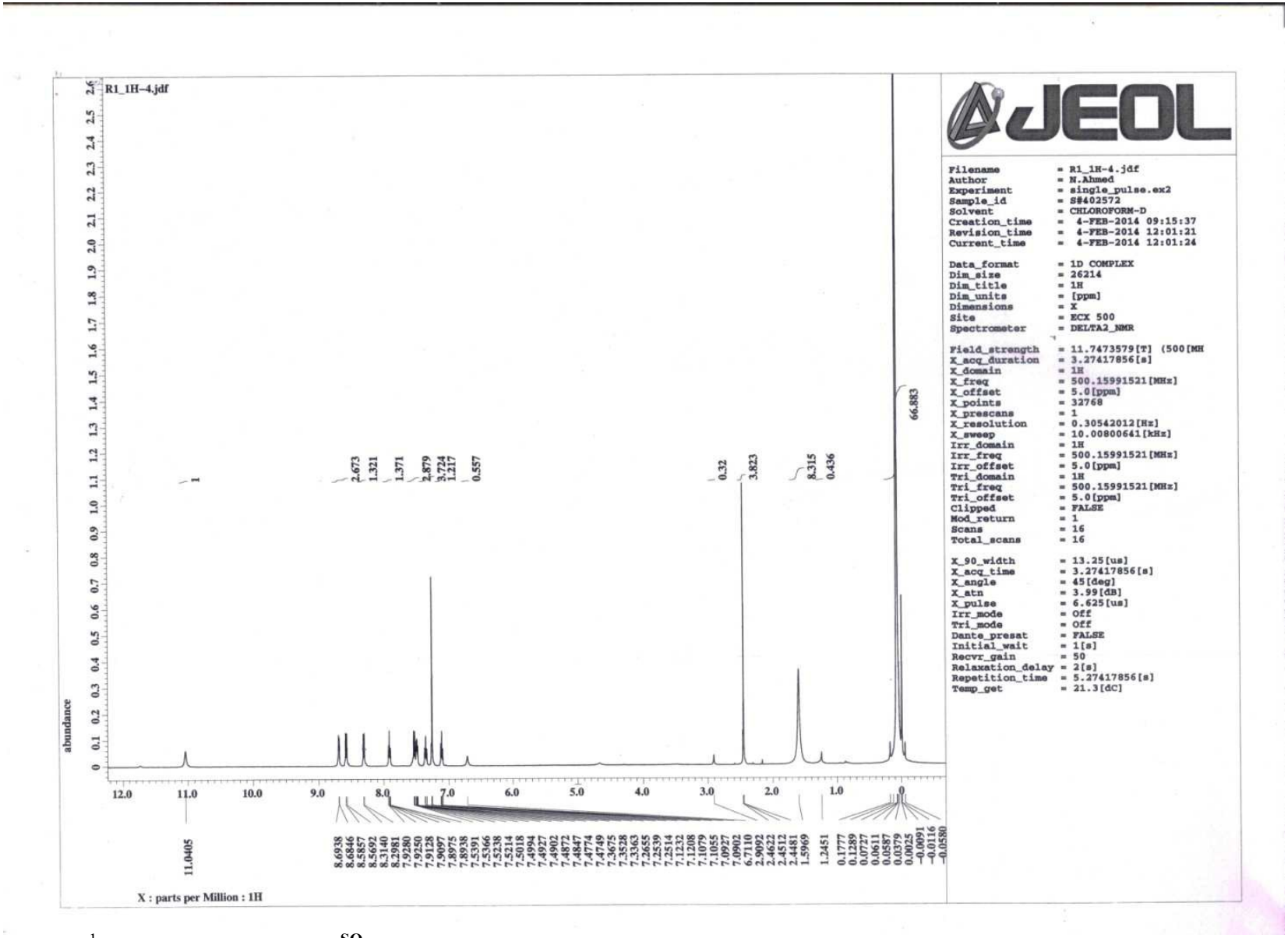

Fig. S4. ^{1}H-NMR spectrum of $\mathbf{L1^{SO}}$ in $CDCl_3$.

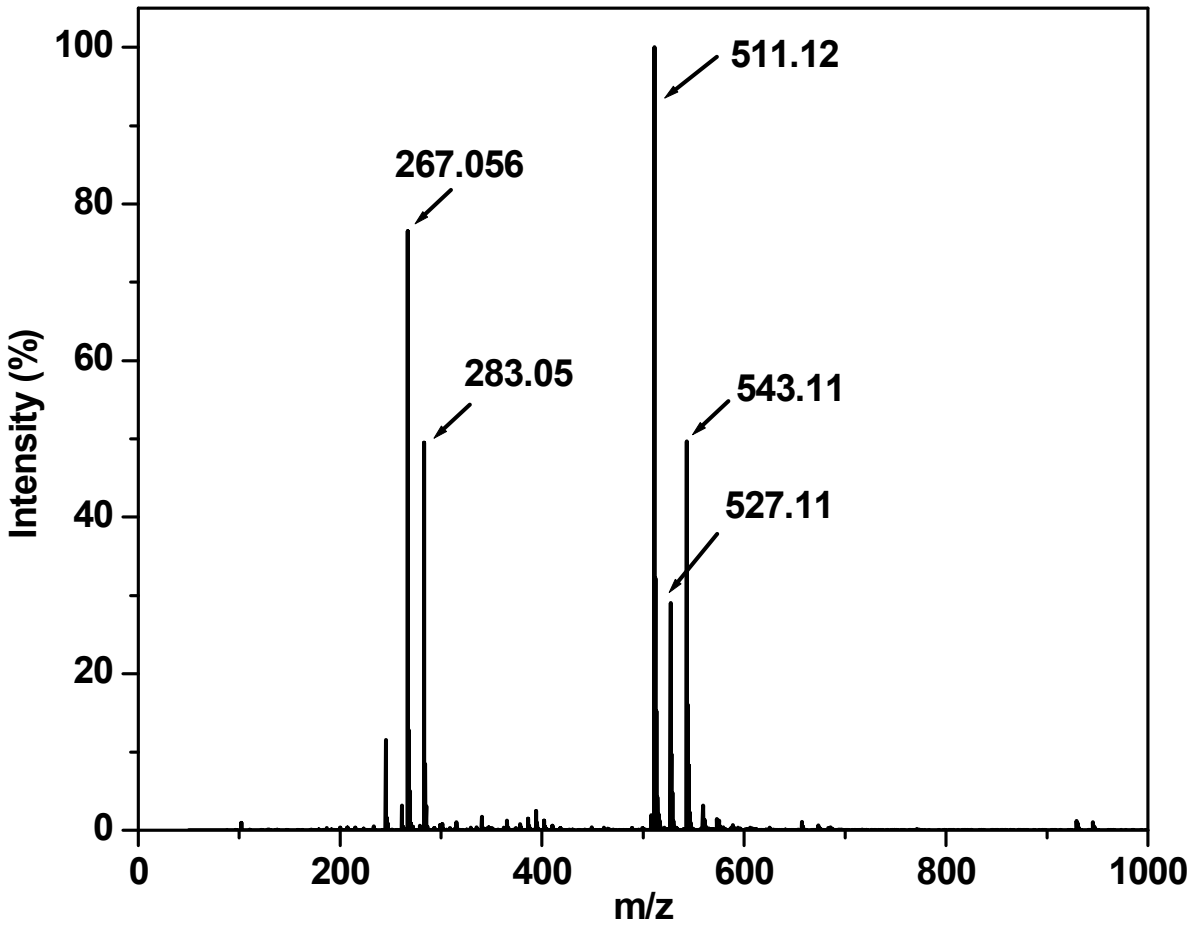

Fig. S5. ESI positive mass spectrum of **HL1^{SO}** taken in $CHCl_3$.

283: {L1^{SO}+ Na}$^+$, 267: {L1^{SO}-O + Na}$^+$, 543: {(L1^{SO})$_2$ + Na}$^+$, 527: {(L1^{SO})$_2$-O + Na}$^+$, 511: {(L1^{SO})$_2$-2O + Na}$^+$

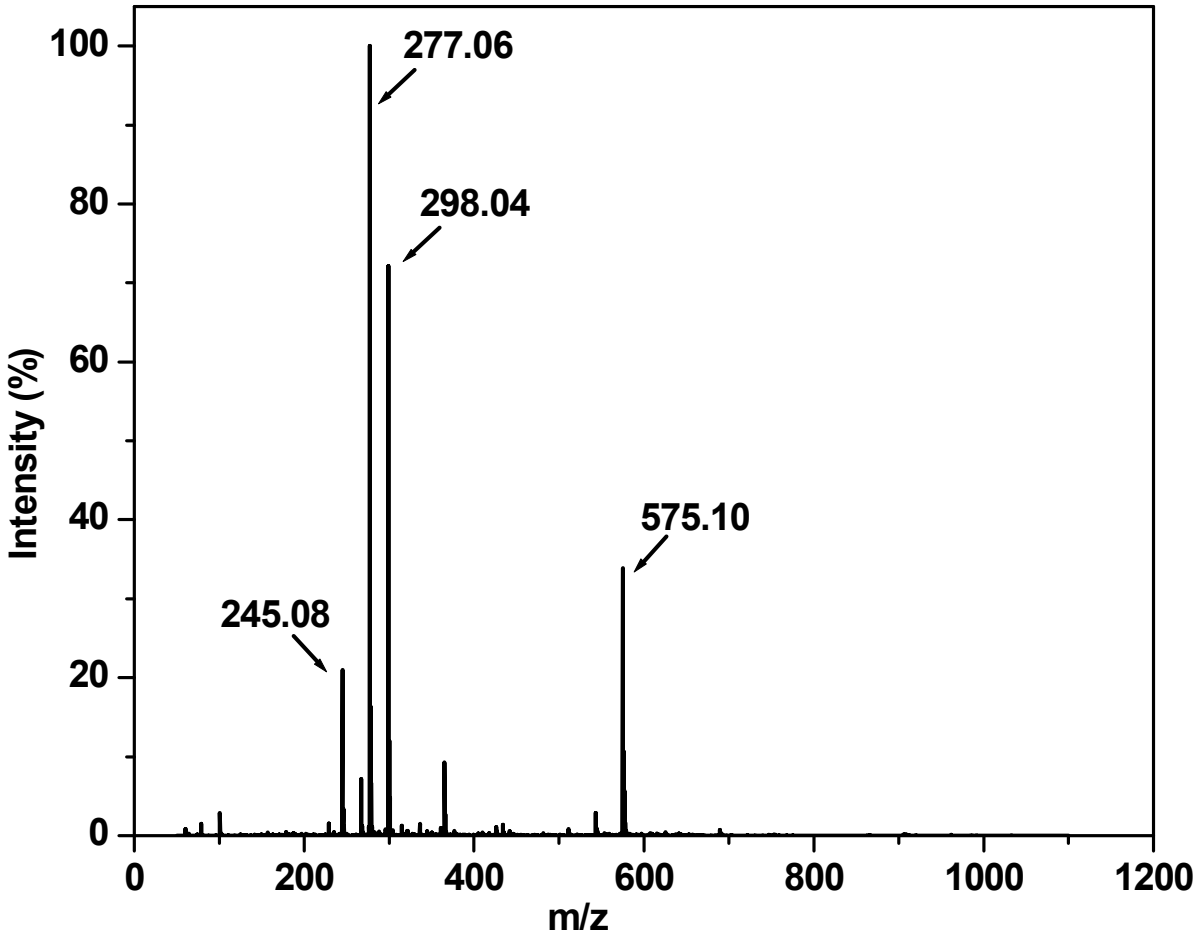

Fig. S6. ESI positive mass spectrum of **HL1^{SO2}** taken in $CHCl_3$.

277: {L1^{SO2}+ H}$^+$, 298: {L1^{SO2} + Na}$^+$, 575: {(L1^{SO2})$_2$ + Na}$^+$, 244: {L1^{SO2}-2O}$^+$

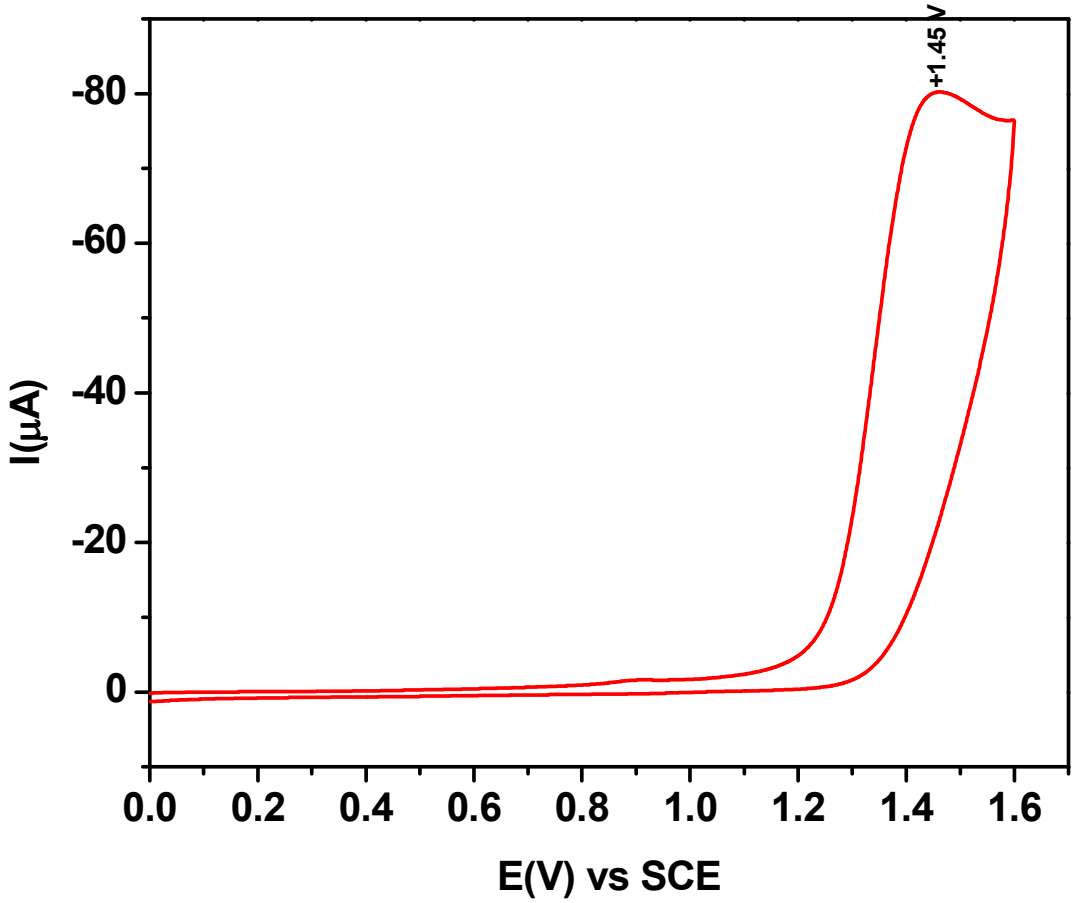

Fig. S7. Cyclic voltammogram of **HL1** in CH_3CN containing $(Bu_4N)ClO_4$ as supporting electrolyte at 298 K at Pt working electrode at a scan rate of 50 mv/s using SCE reference electrode.

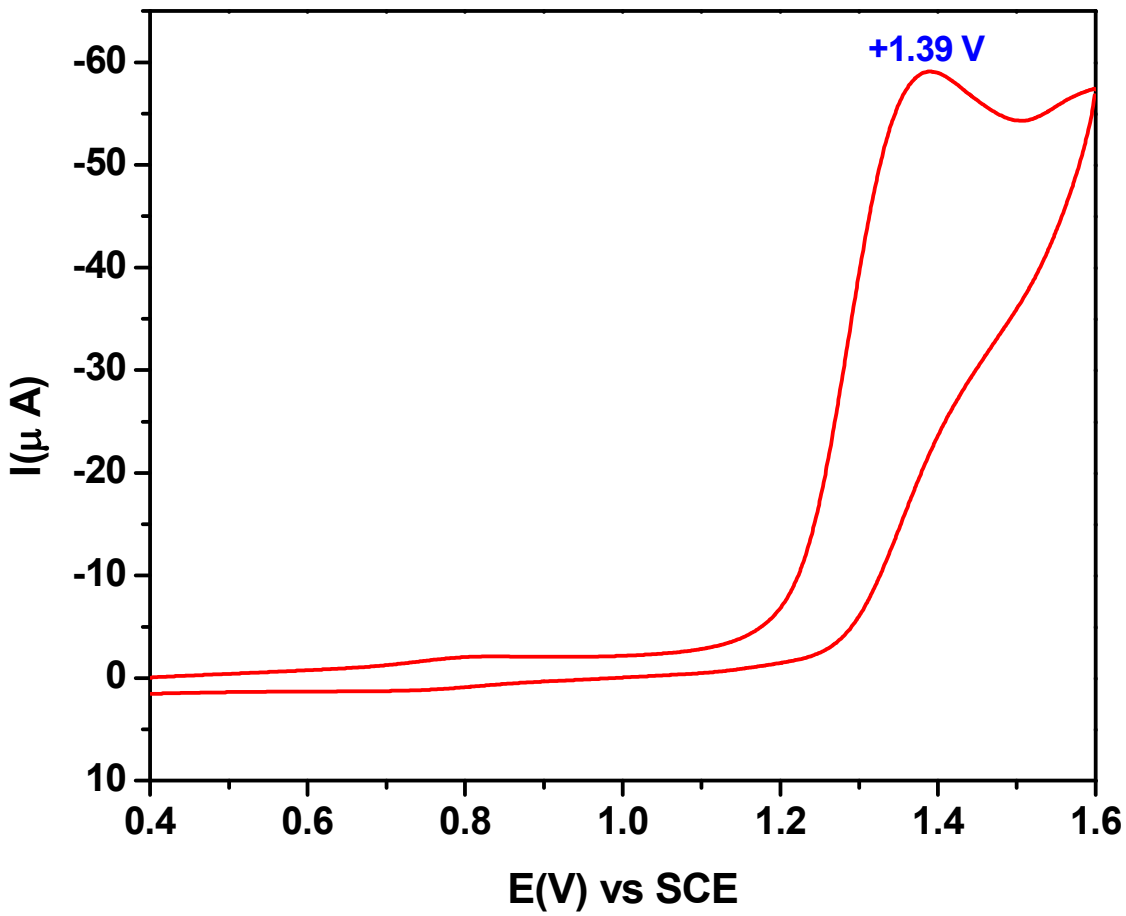

Fig. S8. Cyclic voltammogram of $[(L1)Cu^{II}(NO_3)]$ (**5**) in CH_3CN containing $(Bu_4N)ClO_4$ as supporting electrolyte at 298 K at Pt working electrode at a scan rate of 50 mv/s using SCE reference electrode.

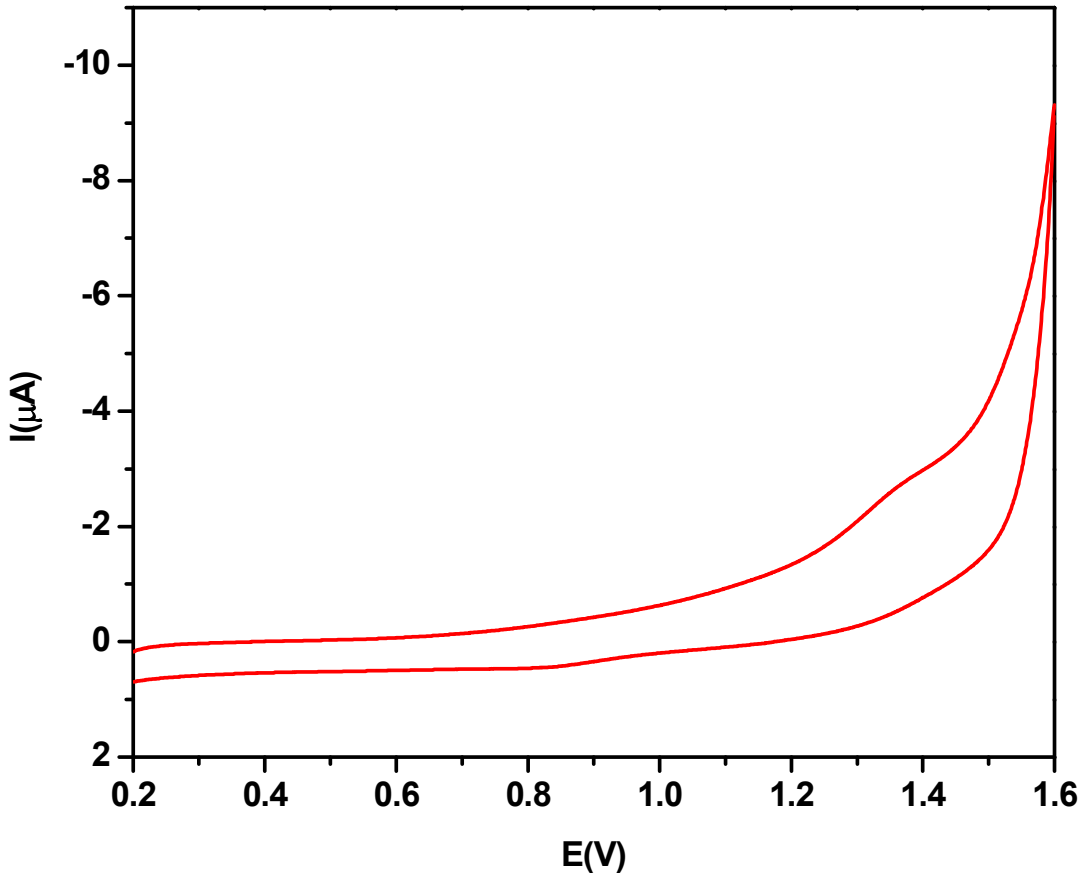

Fig. S9. Cyclic voltammogram of $[(L1^{SO})Cu^{II}(NO_3)]$ (**6**) in CH_3CN containing $(Bu_4N)ClO_4$ as supporting electrolyte at 298 K at Pt working electrode at a scan rate of 50 mv/s using SCE reference electrode.

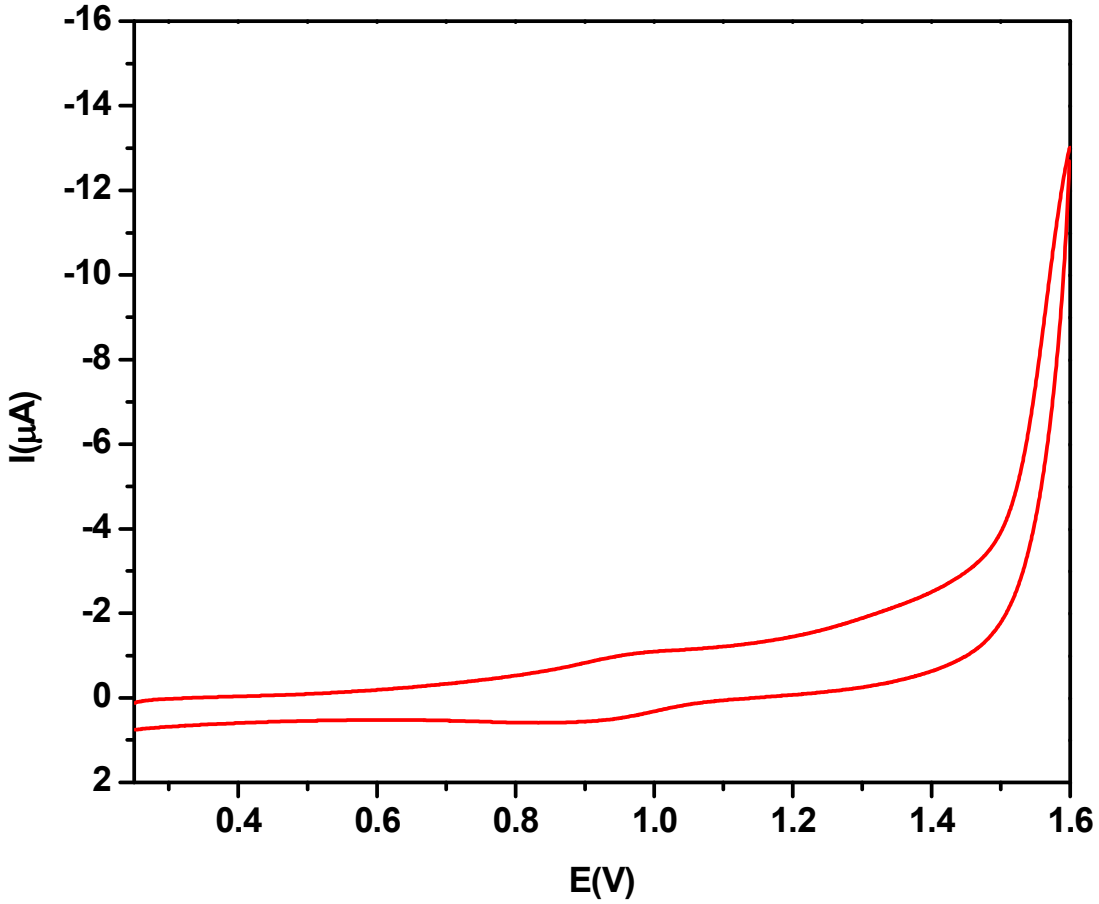

Fig. S10. Cyclic voltammogram of $[(L1^{SO})Cu^{II}(CH_3CN)](ClO_4)$, (**2**) in CH_3CN containing $(Bu_4N)ClO_4$ as supporting electrolyte at 298 K at Pt working electrode at a scan rate of 50 mv/s using SCE reference electrode.

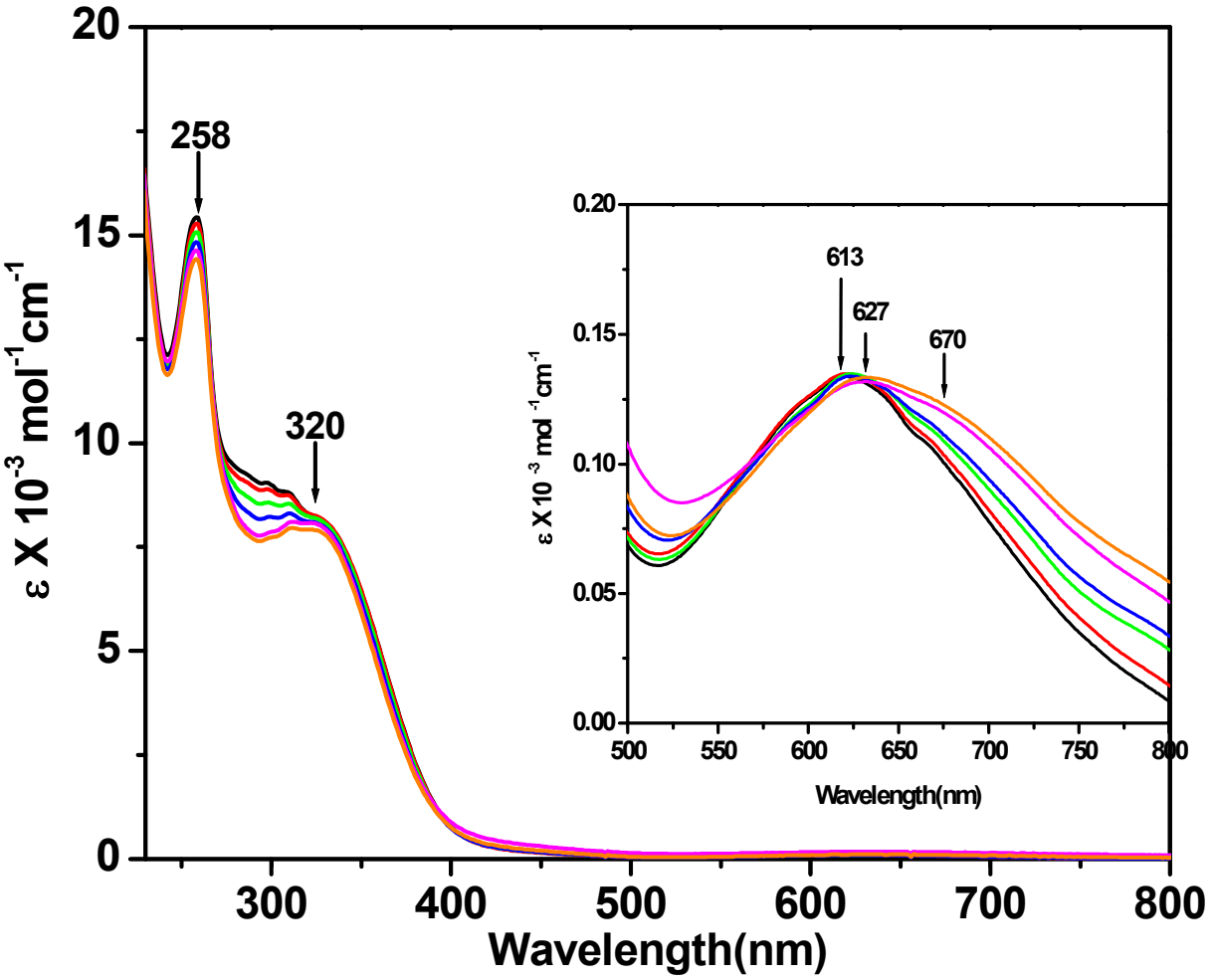

Fig. S 11: Electronic absorption spectral changes when titrating a CH_3CN solution of [(L1)Cu^{II}(ONO)] (**3**) with a CH_3CN solution of one equivalent H_2O_2.

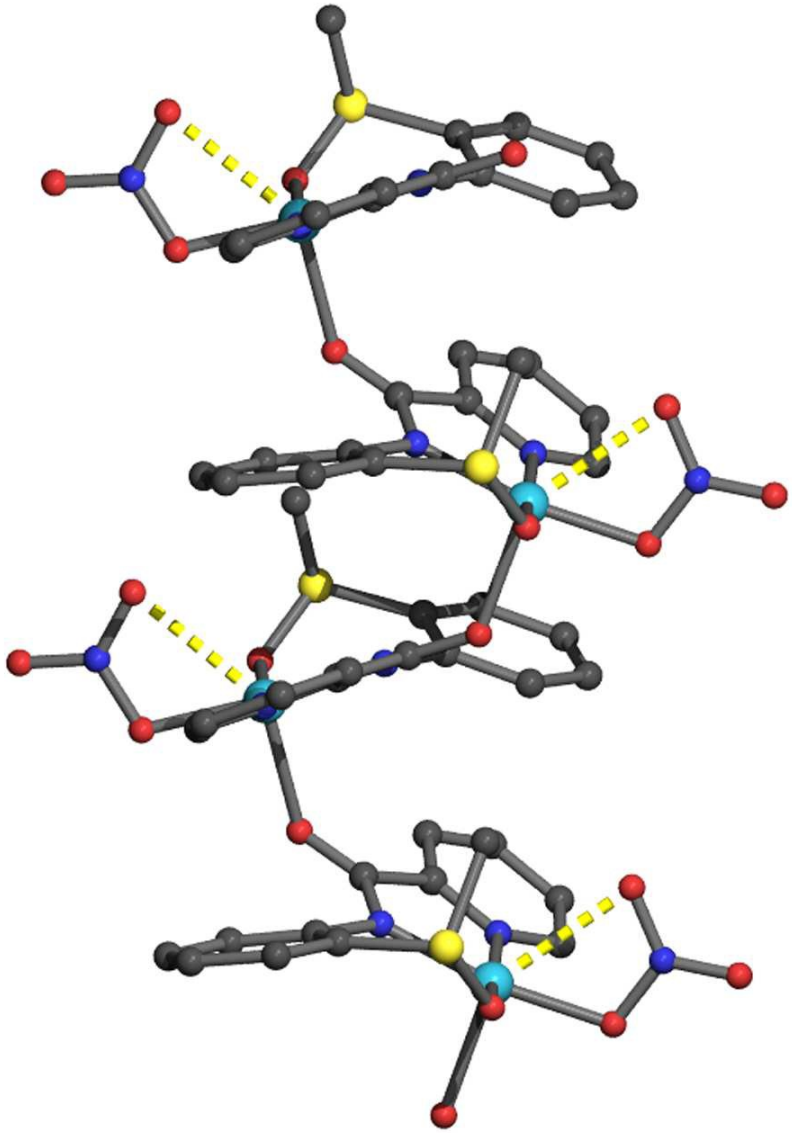

Fig. S12: 3-D Polymeric structure of [($L1^{SO}$)Cu^{II}(NO_3)] (**6**)

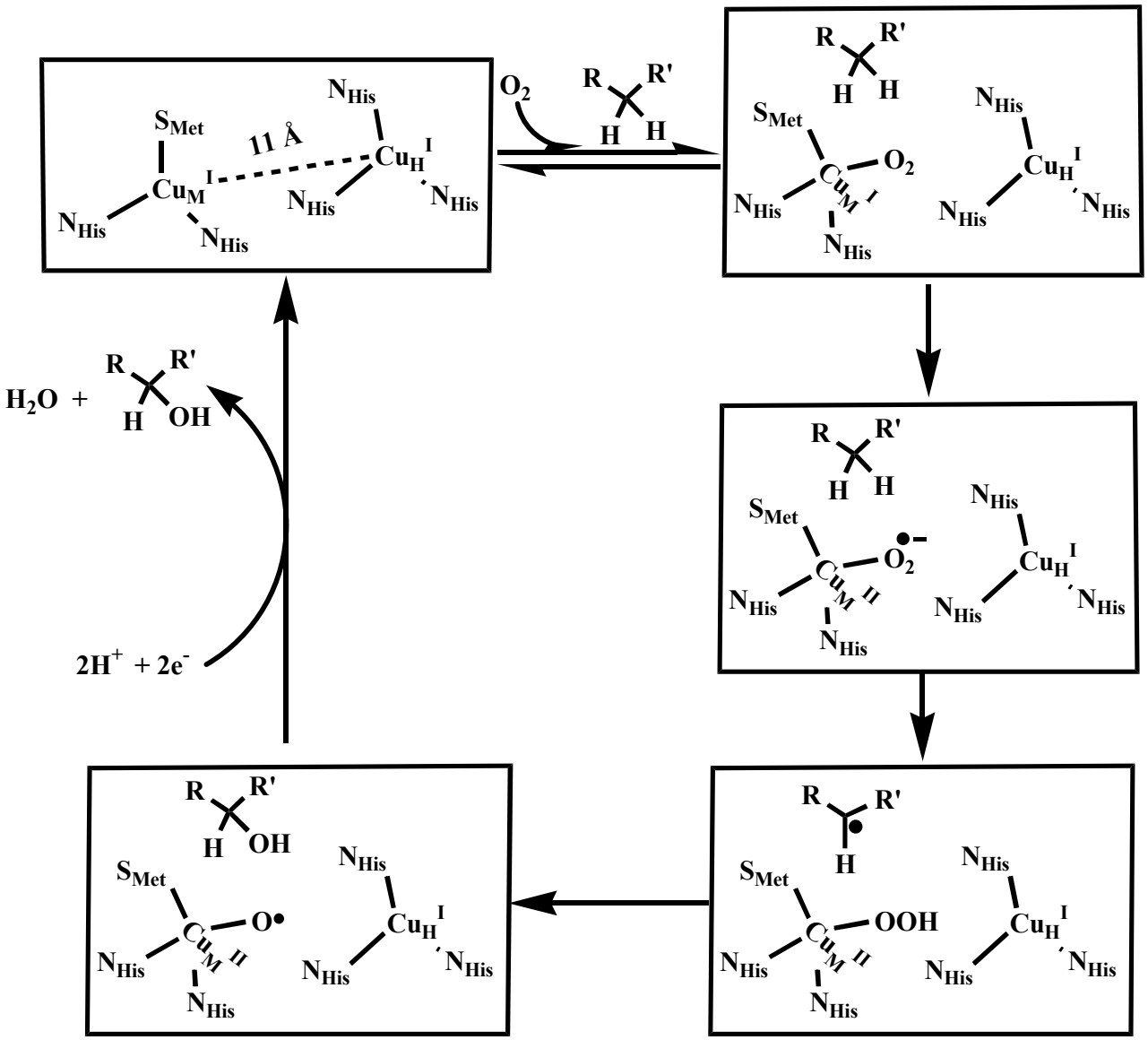

Fig. S13: Proposed mechanistic pathway for C-H hydroxylation, adopted from ref 2(b)

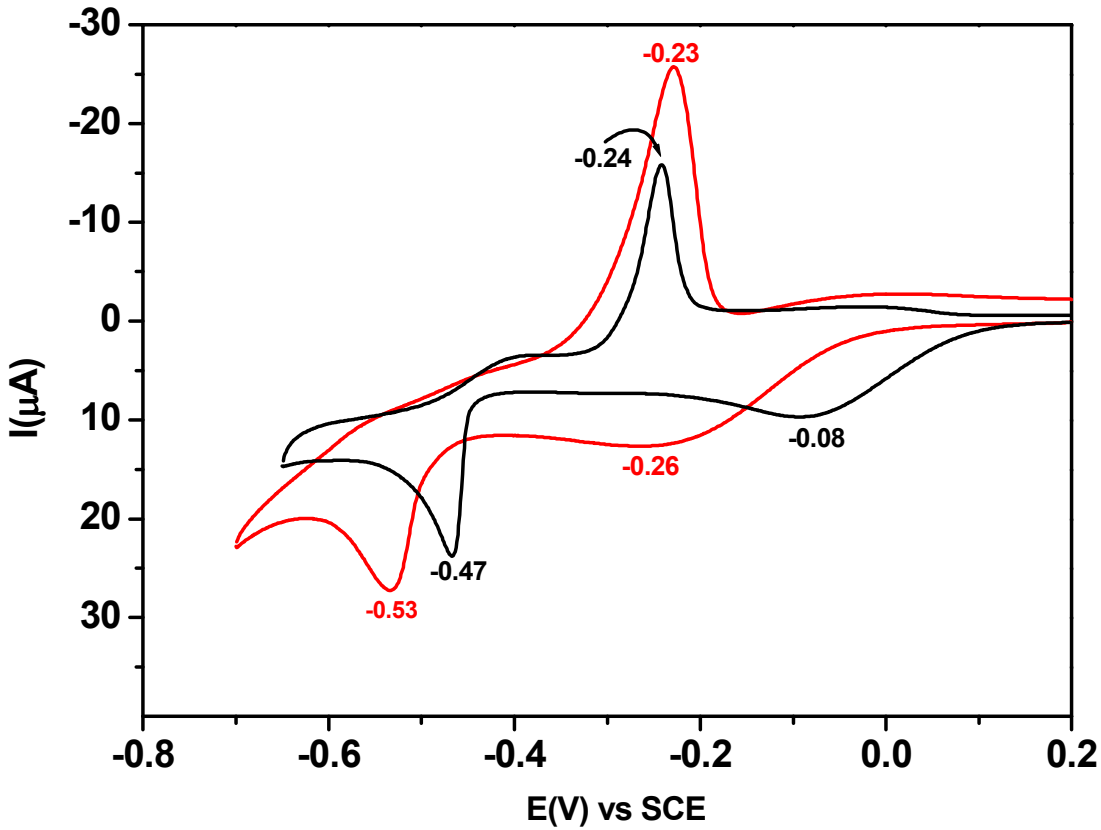

Fig. S14: Cyclic voltammogram of [(L1)$Cu^{II}(NO_3)$] (**5**) (black trace) and (**5** + 40 equiv. $NaNO_3$, red trace) in 1:100 v/v H_2O/CH_3CN mixed solvent containing $(Bu_4N)ClO_4$ as supporting electrolyte at 298 K at Pt working electrode at a scan rate of 50 mv/s using SCE reference electrode.

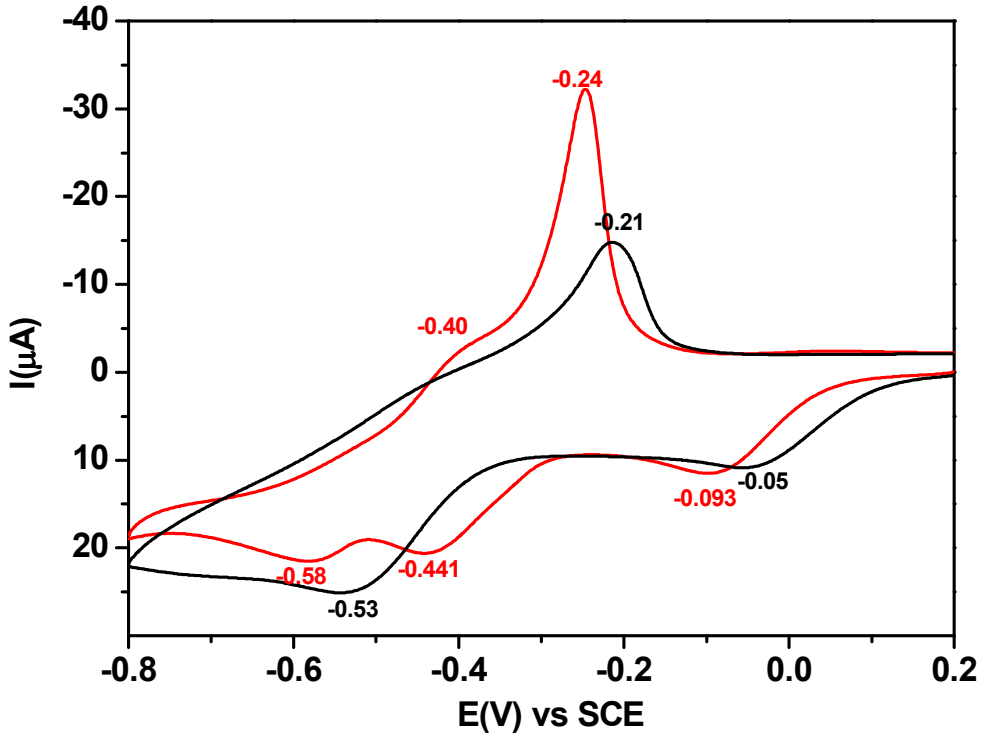

Fig. S15: Cyclic voltammogram of $[(L1^{SO})Cu^{II}(NO_3)]$ (**6**) (black trace) and (**6** + 40 equiv. $NaNO_3$, red trace) in 1:100 v/v H_2O/CH_3CN mixed solvent containing $(Bu_4N)ClO_4$ as supporting electrolyte at 298 K at Pt working electrode at a scan rate of 50 mv/s using SCE reference electrode.

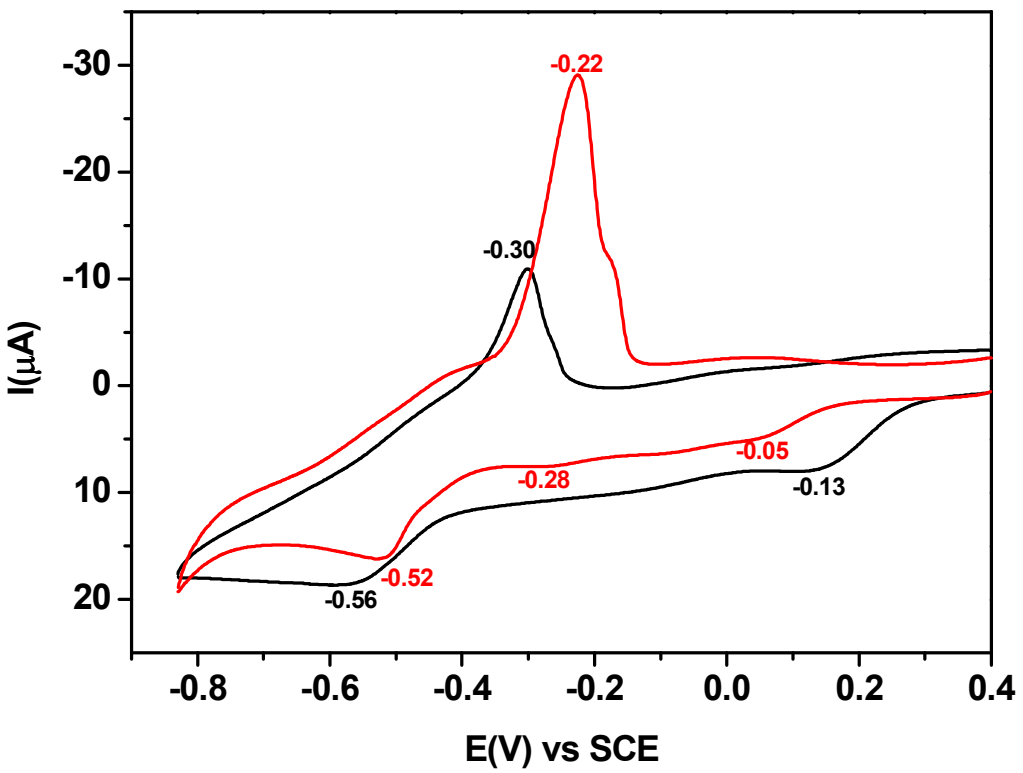

Fig. S16: Cyclic voltammogram of $[(L1^{SO2})Cu^{II}(NO_3)]$ (**7**) (black trace) and (**7** + 40 equiv. $NaNO_3$, red trace) in 1:100 v/v H_2O/CH_3CN mixed solvent containing $(Bu_4N)ClO_4$ as supporting electrolyte at 298 K at Pt working electrode at a scan rate of 50 mv/s using SCE reference electrode.

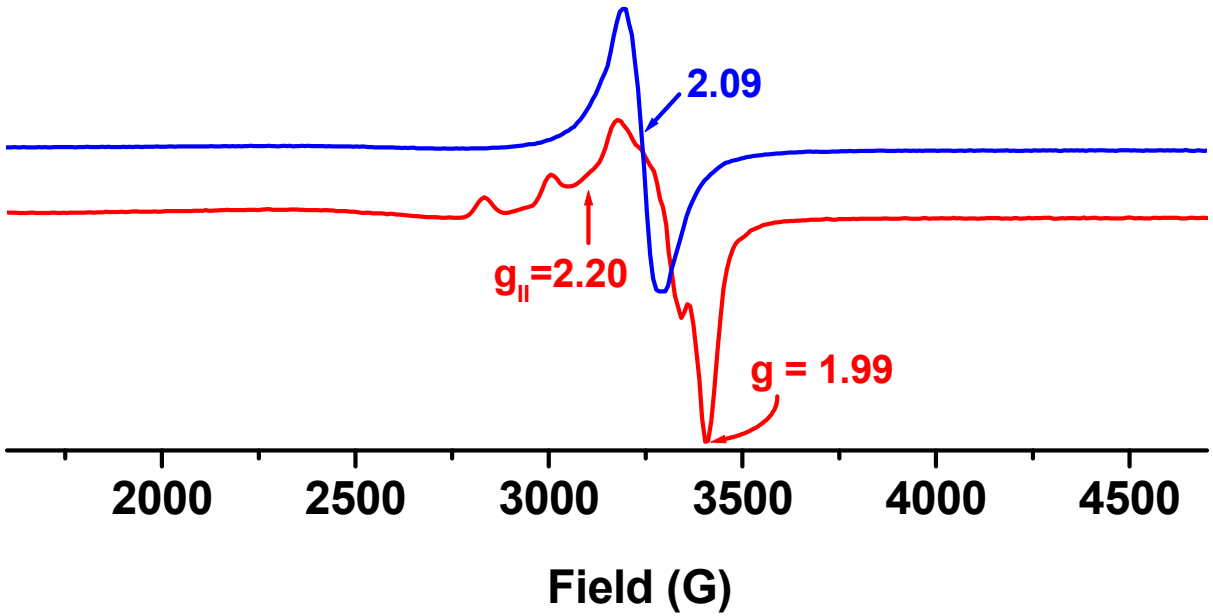

Fig. S17. X-band EPR spectra of [(L1)$Cu^{II}(NO_2)$] (**3**) in MeCN-toluene at 298 K (blue trace) and at 77 K (red trace)

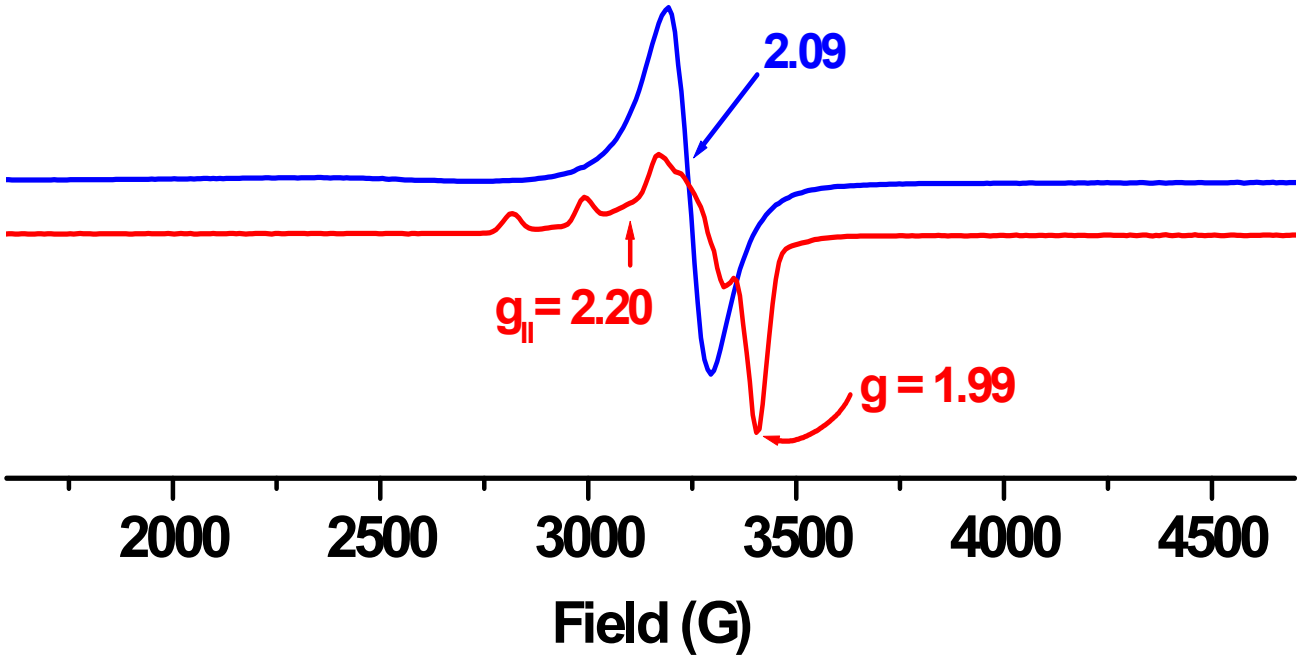

Fig. S18. X-band EPR spectra of [(L1)$Cu^{II}(NO_3)$] (**5**) in MeCN-toluene at 298 K (blue trace) and at 77 K (red trace)

Graphical Abstract:

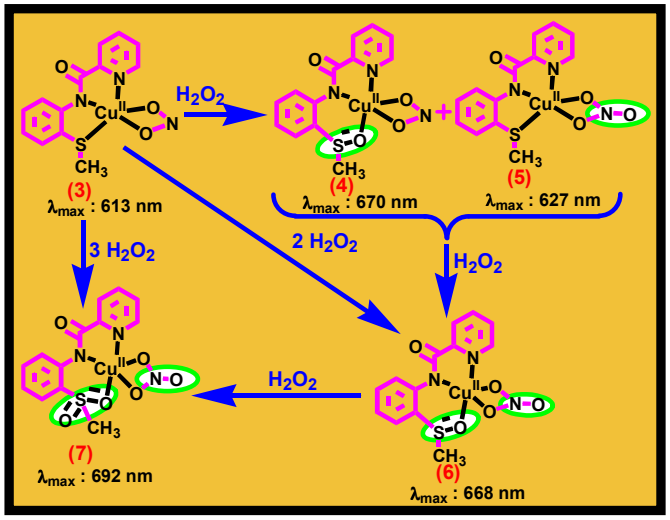

Cu^{II} mediated systematic and stoichiometric oxidation of aryl thioether-S and NO_2^- using oxidants H_2O_2 and molecular O_2.